Atmospheric
Chemistry
and Physics

Global sensitivity of aviation NO_x effects to the HNO_3-forming channel of the $HO_2 + NO$ reaction

K. Gottschaldt[1], C. Voigt[1,2], P. Jöckel[1], M. Righi[1], R. Deckert[1], and S. Dietmüller[1]

[1]Deutsches Zentrum für Luft- und Raumfahrt, Institut für Physik der Atmosphäre, Oberpfaffenhofen, Germany
[2]Johannes-Gutenberg-Universität, Institut für Physik der Atmosphäre, Mainz, Germany

Correspondence to: K. Gottschaldt (klaus-dirk.gottschaldt@dlr.de)

Abstract. The impact of a recently proposed HNO_3-forming channel of the $HO_2 + NO$ reaction on atmospheric ozone, methane and their precursors is assessed with the aim to investigate its effects on aviation NO_x induced radiative forcing.

The first part of the study addresses the differences in stratospheric and tropospheric HO_x-NO_x chemistry in general, by comparing a global climate simulation without the above reaction to two simulations with different rate coefficient parameterizations for $HO_2 + NO \rightarrow HNO_3$. A possible enhancement of the reaction by humidity, as found by a laboratory study, particularly reduces the oxidation capacity of the atmosphere, increasing methane lifetime significantly. Since methane lifetime is an important parameter for determining global methane budgets, this might affect estimates of the anthropogenic greenhouse effect.

In the second part aviation NO_x effects are isolated independently for each of the three above simulations. Warming and cooling effects of aircraft NO_x emissions are both enhanced when considering the HNO_3-forming channel, but the sum is shifted towards negative radiative forcing. Uncertainties associated with the inclusion of the $HO_2 + NO \rightarrow HNO_3$ reaction and with its corresponding rate coefficient propagate a considerable additional uncertainty on estimates of the climate impact of aviation and on NO_x-related mitigation strategies.

1 Introduction

Aircraft emissions of reactive nitrogen oxides ($NO_x = NO + NO_2$) peak in the upper troposphere and lower stratosphere (UTLS), and the resulting NO_x increase impacts on the radiatively active trace gases ozone (O_3), methane (CH_4) and stratospheric water vapour. The radiative forcing of aircraft induced O_3 is one of the largest contributions to aviation climate impact, comparable to that of CO_2 (Lee et al., 2009). However, when determining the net effect of NO_x emissions a number of tradeoffs between the O_3 component and other NO_x induced effects have to be understood for a sufficiently reliable assessment. The necessity of a thorough understanding becomes even more important, if the more complicated tradeoff effects between NO_x emissions and other aviation effects (CO_2, contrails) arising from changes in aircraft engine design or flight operation have to be considered in attempts to reduce the total climate impact of aviation. Yet, the level of scientific understanding of the aviation NO_x contribution to anthropogenic climate forcing has been judged as moderate to poor (Lee et al., 2009, 2010; Holmes et al., 2011). This judgement did not include the possible effects of the proposed $HO_2 + NO \rightarrow HNO_3$ reaction (Butkovskaya et al., 2005, 2007, 2009; Chen et al., 2009).

The concentration of ozone in the UTLS is determined by transport, mixing and by chemical processes, mainly the ozone destroying, catalytic peroxy radical ($HO_x = HO_2 + OH$) and halogen radical cycles in concert with reactions involving reactive nitrogen oxides (Wennberg et al., 1998). Adding (aviation) NO_x to the chemical system and considering gas phase chemistry only, the effect on ozone changes sign in the altitude range of 12 to 25 km (Kawa et al., 1998;

Penner et al., 1999; Søvde et al., 2007; Köhler et al., 2008; Fichter, 2009). Above that altitude region of zero net effect, aircraft NO$_x$ emissions intensify the NO$_x$ cycle, enhancing catalytic ozone destruction. This cycle operates more efficiently higher up in the stratosphere, because peroxy radicals (sequestering NO$_x$ into reservoir species such as nitric acid, HNO$_3$) and NO$_2$ photolysis are less important at higher altitudes. Below that region, the ozone destroying NO$_x$ cycle is bypassed via peroxy radicals, and direct emissions of NO$_x$ by aircraft can lead to increased ozone production by reducing the abundance of HO$_x$ molecules. Furthermore, the rates of the major net loss reactions of peroxy radicals, as well as ozone production, all depend nonlinearly and even non-monotonically on NO$_x$ levels (Ehhalt and Rohrer, 1994). However, such chemical nonlinearities are expected to be small for the atmospheric response to aircraft emissions (Grewe et al., 2002; Holmes et al., 2011).

Methane is emitted from the Earth's surface and lost in the troposphere mainly by the reaction with OH. Thus NO$_x$ emissions affect methane life time via OH. Methane perturbations in turn have an effect on ozone (Ehhalt et al., 2001). Methane oxidation is also a major source of stratospheric water vapour.

Beyond these well-known reactions, the effects of NO$_x$ emissions may be further affected by (i) the uptake of HNO$_3$ into ubiquitous super-cooled aerosol particles, in particular in the stratosphere (Fahey et al., 1993; Schreiner et al., 1999; Voigt et al., 2000), or into ice (e.g. Voigt et al., 2006, 2007; Kärcher and Voigt, 2006), but also by (ii) the recently discovered HNO$_3$-forming channel of the HO$_2$ + NO reaction (Butkovskaya et al., 2005, 2007; Chen et al., 2009):

$$HO_2 + NO \rightarrow NO_2 + OH \tag{R1a}$$

$$HO_2 + NO(+M) \rightarrow HNO_3(+M) \tag{R2a}$$
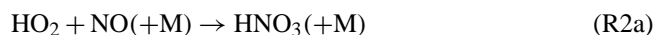
with the rate coefficients k_{1a} and k_{2a}, respectively. Butkovskaya et al. (2009) supposed that HO$_2$ + NO forms the HOONO intermediate complex that mostly decomposes into OH + NO$_2$. A small fraction forms nitric acid, possibly involving another molecule (M).

An enhancement of HNO$_3$ formation in the presence of water has been measured in the laboratory for the range of 0–70 % relative humidity with respect to liquid water (Butkovskaya et al., 2009). The enhancement of HNO$_3$ formation in the presence of water vapour may be due to the formation of an H$_2$O·HO$_2$ complex:

$$H_2O + HO_2 \leftrightarrow H_2O\cdot HO_2 \tag{R3}$$

suggesting the following chemical mechanism instead of Reactions (R1a) and (R2a):

$$H_2O\cdot HO_2 + NO \rightarrow OH + NO_2 + H_2O \tag{R1b}$$

$$H_2O\cdot HO_2 + NO \rightarrow HNO_3 + H_2O \tag{R2b}$$
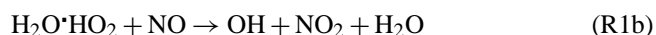
The effects of Reaction (R2a) on atmospheric composition have been studied before (Brühl et al., 2007; Cariolle et al., 2008; Søvde et al., 2011), accounting for pressure and temperature dependence of k_{2a}. We additionally considered that both reaction channels may be modified in the presence of water vapour. The combinations of Reactions (R1a) with (R2a) and of (R1b) with (R2b) are two alternative formulations for the net reaction of HO$_2$ with NO, forming NO$_2$, OH and HNO$_3$. For the sake of readability, the HNO$_3$-forming channel in general (R2a or R2b) is denoted by (R2), whereas (R1) indicates the other channel (R1a or R1b). Likewise, k_2 refers to k_{2a} or k_{2b}, and k_1 to k_{1a} or k_{1b}.

We note that Reaction (R2) is not generally accepted yet, according to IUPAC (2008): "Although the possibility for HNO$_3$ formation via rearrangement of an initially formed HOONO adduct has been confirmed in the theoretical study of Zhang and Donanhue (2006), further studies of the formation of HNO$_3$ in the title reaction are urgently required to reduce uncertainties", and according to Sander et al. (2011): "Until the results have been confirmed by other groups and are better understood, no recommendation can be made".

Unger (2011) reported a negligible impact of (R2a) on short-lived ozone perturbations due to aviation NO$_x$. Søvde et al. (2011) investigated the response of ozone and methane to the difference between pre-industrial and modern emissions of ozone precursors (NO$_x$, CH$_4$, CO, NMHC) with and without Reaction (R2a), but they did not separate out the effects of NO$_x$ emissions. In this paper we demonstrate the potential importance of (R2) for assessing the climate impact of aviation NO$_x$, when considering radiative forcing (RF) from perturbations in ozone and methane. The results emphasize the need for further experimental data on the rate coefficient for Reaction (R2) that are valid in the entire range of atmospheric temperatures, pressures, and water vapour concentrations.

The paper is organized as follows: Sect. 2 describes the base model configuration and the changes to the chemical mechanism when including Reaction (R2) for sensitivity simulations. The results of the base simulation and of two sensitivity simulations with different rate coefficients are presented in Sect. 3. All three simulations are repeated with aircraft NO$_x$ emissions switched off exclusively, to isolate the perturbations from aviation. Chemical effects of aviation NO$_x$ are discussed in Sect. 4, and Sect. 5 deals with the corresponding radiative forcings. Finally, Sect. 6 provides a discussion of our results and the conclusions.

2 Methodology

2.1 Base model configuration, no additional HNO$_3$ forming channel

This study is based on the global ECHAM/MESSy Atmospheric Chemistry (EMAC) model. EMAC is a numerical

chemistry and climate simulation system that includes submodels describing tropospheric and middle atmosphere processes and their interaction with oceans, land and human influences (Jöckel et al., 2006). It uses the first version of the Modular Earth Submodel System (MESSy1, Jöckel et al., 2005) to link multi-institutional computer codes. The core atmospheric model is the 5th generation European Centre Hamburg general circulation model (ECHAM5, Roeckner et al., 2003, 2006). For the present study EMAC (ECHAM5: version 5.3.01, MESSy: modified version 1.10) is applied in the T42L90MA-resolution, i.e. with a spherical truncation of T42 (corresponding to a quadratic Gaussian grid of approx. 2.8 by 2.8 degrees in latitude and longitude) with 90 vertical hybrid pressure levels up to 0.01 hPa. The model setup comprised the submodels listed in Table B1.

EMAC is operated in Quasi Chemistry Transport Model (QCTM) mode (Deckert et al., 2011), providing identical dynamics for the chemical calculations in all simulations (see Appendix A). Dynamics in the free troposphere (up to about 200 hPa) is nudged towards the analysed ECMWF meteorology. This is inherited from the "S2" setup of Jöckel et al. (2006), which was shown to result in most realistic atmospheric dynamics, compared to other nudging settings. Gravity wave forcing is treated as in S2, and clouds with a standard EMAC scheme (Sundqvist, 1978; Lohmann and Roeckner, 1996). All simulations cover two years and are nudged to the synoptic meteorological conditions of the years 2000 and 2001.

Gas phase chemistry is calculated with the MECCA1 chemistry submodel (Sander et al., 2005), consistently from the surface to the stratosphere. The applied chemical mechanism included full stratospheric complexity, but neglected the sulphur and halogen families in the troposphere. It has been evaluated by Jöckel et al. (2006), showing that it is a reasonably realistic representation of atmospheric chemistry. A temperature-dependent rate coefficient,

$$k_0 = k_1 + k_2 = A \cdot \exp\left(-\frac{B}{T}\right) \tag{1}$$

is assumed for the HO$_2$ + NO conversion via both reaction pathways (R1 and R2). All simulations for this paper are carried out with the Arrhenius factor $A = 3.5 \times 10^{-12}$ cm^3 s^{-1}, and activation temperature $B = 250$ K (Sander et al., 2003). Temperature T is in K. The base simulation had $k_1 = k_0$ for Reaction (R1), and Reaction (R2) was switched off, i.e. $k_2 = 0$.

The initial chemical mixing ratios stem from output on 31 December 1999 of a previous simulation with the chemistry mechanism as in Jöckel et al. (2006). The first year was discarded as chemical spin-up time. Aircraft emissions included NO$_x$ only, emitted as 1.815 Tg(NO) yr^{-1}. Further details about the model configuration are summarized in Appendix B.

2.2 Sensitivity simulations with HNO$_3$ forming channel, no humidity modification

These simulations differ from the base simulation in the definition of k_1 and k_2:

$$k_{2a} = \frac{k_0 \cdot \beta}{1 + \beta} \tag{2}$$

$$k_1 = k_0 - k_2 \tag{3}$$

i.e. $k_{1a} = k_0 - k_{2a}$ or $k_{1b} = k_0 - k_{2b}$. Butkovskaya et al. (2007) proposed

$$\beta(p, T) = 0.01 \cdot \left(\frac{530}{T} + p \cdot 4.8 \times 10^{-6} - 1.73\right) \tag{4}$$

with pressure p in Pa and T in K. Equation (4) is based on an empirical fit to laboratory data and is valid for dry conditions, in the pressure range 93–800 hPa and the temperature range 223–298 K. Consequently both reaction rates depend on temperature and pressure in this case. Brühl et al. (2007) applied Eq. (4) for atmospheric conditions up to a pressure altitude of 0.01 hPa, and concluded that it brings nitric acid in the upper atmosphere of EMAC into better agreement with MIPAS observations. We adopted Eq. (4) like Brühl et al. (2007), although Butkovskaya et al. (2009) stated that β remains uncertain at low pressure and requires further experimental work. The focus of our study is on the UTLS, which is well within the claimed validity range of Eq. (4).

2.3 Sensitivity simulations with HNO$_3$ forming channel, with humidity modification

By fitting the enhancement factor of HNO$_3$ formation as a function of H$_2$O concentration, Butkovskaya et al. (2009) derived the ratio $\gamma = k_{2b}/k_{2a}$ at 298 K and 267 hPa. Then, humidity effects can be considered as a modification of Eq. (2):

$$k_{2b} = \frac{k_0 \cdot \beta \cdot (1 + \gamma \cdot \alpha)}{(1 + \beta) \cdot (1 + \alpha)} \tag{5}$$

Butkovskaya et al. (2009) infer that the effect of water vapour on HNO$_3$ formation depends only weakly on pressure in the range of 133 to 933 hPa, while the temperature dependence is unknown (LeBras, 2011). A constant factor $\gamma = 42$ (Adams, 1979; Butkovskaya et al., 2009) is assumed in the simulations featuring Reaction (R2b) (and thus k_{2b}). Equation (5) allows us to build on the representation of (R1a) and (R2a) in the code, instead of explicitly implementing Reactions (R3), (R1b) and (R2b). The term

$$\alpha = c_{H_2O} \cdot K_{eq} \tag{6}$$

depends on the equilibrium coefficient (in cm^3)

$$K_{eq} = 6.6 \times 10^{27} \cdot T \cdot \exp\left(\frac{3700}{T}\right) \tag{7}$$

Table 1. Simulations performed for this study. They differ only in the rate coefficient for the HNO$_3$-forming channel of HO$_2$ + NO (Reaction R2) and aircraft NO$_x$ emissions. The rate coefficient k_2 is either zero (**B**ase), depended on pressure and temperature (**D**ry), or additionally on water vapour concentration (**W**et). **A**viation is on (**A**) or zero (**0**). Each pair of simulations with identical treatment of (R2) defines a sensitivity block (ΔB: BA vs. B0, ΔD: DA vs. D0, ΔW: WA vs. W0) for the discussion of aviation NO$_x$ effects in the corresponding chemical regime. The annual mean ozone burden $\langle[O_3]\rangle$ is calculated from the surface to 0.01 hPa.

Simulation	BA	B0	DA	D0	WA	W0
Sensitivity block	ΔB		ΔD		ΔW	
Rate coefficient for (R2)	$k_2 = 0$		$k_2(p, T)$		$k_2(p, T, c_{H_2O})$	
Aircraft NO$_x$ emissions	on	off	on	off	on	off
$\langle[O_3]\rangle$, in DU	316.12	315.62	314.59	314.06	310.29	309.72

of Reaction (R3) (Kanno et al., 2006) and on the molecular concentration of water, c_{H_2O} in cm^{-3}.

The total rate coefficient $k_0 = k_1 + k_2$ of the HO$_2$ + NO reaction does not depend on c_{H_2O} in this formulation, consistent with Bohn and Zetzsch (1997).

2.4 Interpretation of sensitivity simulations

Six simulations are discussed in this study that all share the same meteorology, but differ in their atmospheric chemistry setup (Table 1). The **B**ase simulation without (R2), and with **A**ircraft emissions (BA) serves as reference for the comparison to simulations DA (**D**ry = rate coefficient for Reaction (R2a) according to Eq. (2), with **A**ircraft emissions) and WA (**W**et = rate coefficient for (R2b) with humidity modification according to Eq. (5), with **A**ircraft emissions). Any pair of a reference and a sensitivity simulation is denoted as "sensitivity block". The sensitivity blocks (BA versus DA) and (BA versus WA) are discussed to isolate the effects of (R2) on atmospheric HNO$_3$, HO$_x$, NO$_x$ and O$_3$ background mixing ratios.

Each of the above simulations represents a different chemical atmospheric chemical regime, but all three have identical emissions. Thus three more reference simulations are needed to isolate aviation NO$_x$ effects by pairs. B0 (**B**ase simulation, **0** = zero aircraft emissions) is compared to BA. D0 and W0 serve as reference cases for the sensitivities DA and WA, respectively. The corresponding sensitivity blocks are denoted ΔB, ΔD and ΔW.

Sensitivity method: we evaluate deviations of a simulation with aircraft NO$_x$ emissions from one without. The response to the perturbation may weakly depend on background NO$_x$ mixing ratios. Aircraft NO$_x$ emissions change the NO$_x$ background and therefore affect their own effects. Furthermore, buffering in the chemical system may partially compensate the effects of switched-off emissions (Grewe et al., 2012). Thus the sensitivity method is inappropriate for source attribution, but well suited to evaluate the atmospheric impact of changed emissions (Grewe et al., 2010). We refer to the differences between otherwise identical simulations with and without aviation NO$_x$ as "effects of aviation NO$_x$". The term is ambiguous though and may have a different phys-

ical meaning with other methodologies, e.g. tagging. Since we only apply the sensitivity method, "effects of ..." is still used throughout the paper for brevity. The sensitivity method shows the net response of the chemical system to a perturbation, including all chemical nonlinear and buffering effects without discrimination. It is discussed for sensitivity blocks ΔB, ΔD and ΔW how each hypothetical atmosphere would change without aircraft NO$_x$ emissions.

3 Effects of the HO$_2$ + NO → HNO$_3$ reaction on atmospheric chemistry

In this section we discuss how Reactions (R2a) or (R2b) (summarized as R2) affect background atmospheric chemistry, without considering aviation effects. Two simulations (DA, WA) with different reaction rate coefficients for (R2) are compared to a reference simulation (BA) without (R2). All three simulations have identical meteorology and identical emissions, including aviation.

The left column of Fig. 1a/b shows the 12-month average of zonal mean mixing ratios of HNO$_3$, OH, NO$_x$ and O$_3$ for simulation BA. Mixing ratios of trace gas X are denoted [X] in the following text. Absolute (WA-BA) and relative (100{WA-BA}/BA) deviations of annual zonal mean [HNO$_3$], [NO$_x$], [OH], and [O$_3$] of WA with respect to BA are shown in the middle and right columns of Fig. 1a/b, respectively. Differences to simulation DA are discussed in the text but not shown.

In an attempt to check if any of the chemical regimes yields unrealistic results, [HNO$_3$], [NO$_x$], [CO] and [O$_3$] profiles from simulations BA, DA and WA are compared to observational profiles of Emmons et al. (2000). However, all simulations match the observed trace gas mixing ratios well (see Supplement, Figs. S1–S4). Neither the regime without the HNO$_3$-forming channel of HO$_2$ + NO, nor the two regimes with it can be ruled out according to this test.

Reaction (R2a) is favoured at low temperatures and high pressures. This causes a local maximum in the cold spot of the tropical UTLS, where about 1 % of the HO$_2$ + NO reaction proceed via the HNO$_3$ forming channel (see Supplement, Fig. S5). Humidity is highest near the surface,
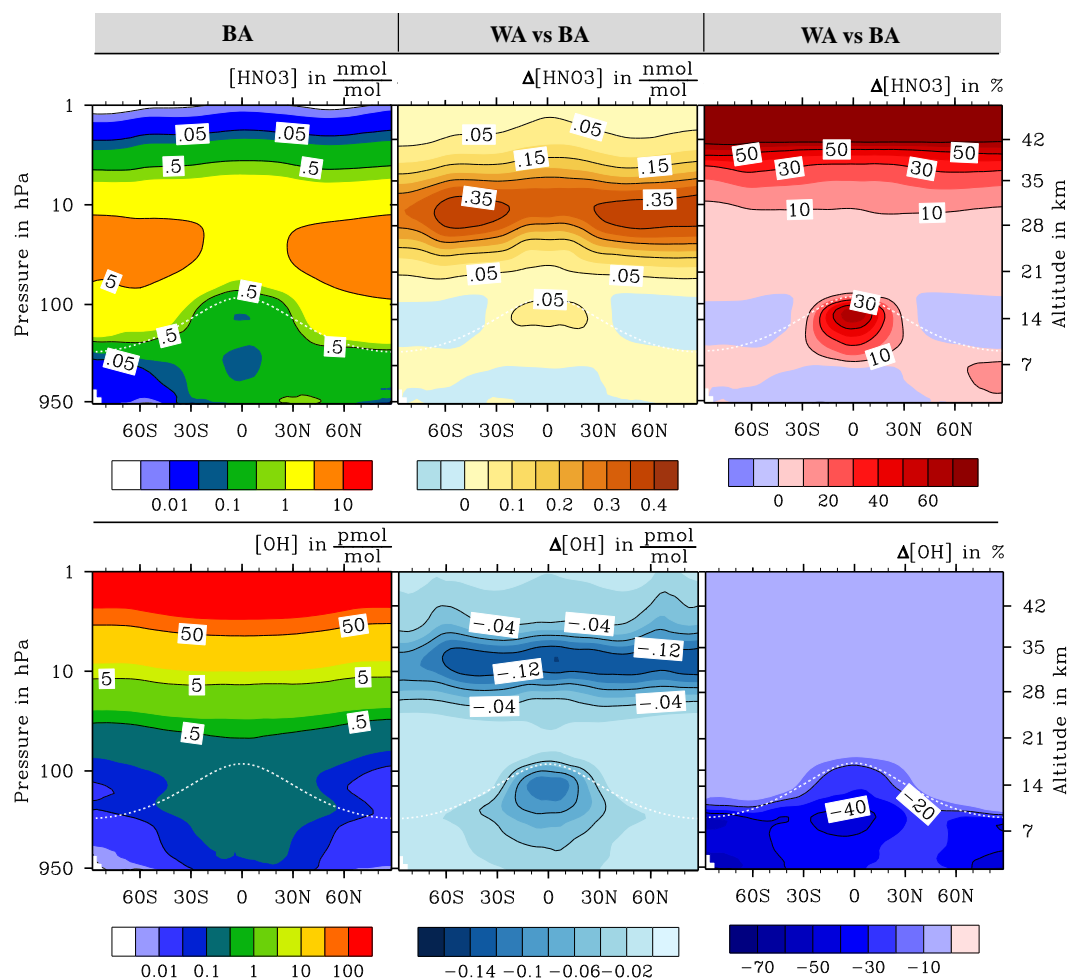
Fig. 1a. Comparison of [HNO$_3$] and [OH] in a simulation with the HNO$_3$-forming channel to a reference simulation without HO$_2$ + NO $\rightarrow$ HNO$_3$. Both simulations have identical aviation NO$_x$ emissions. The left column shows annual zonal mean mixing ratios in the reference simulation (BA). The middle and right columns show absolute (WA-BA) and relative ($100 \cdot \frac{\text{WA}-\text{BA}}{\text{BA}}$) deviations when including the HNO$_3$-forming channel with a rate coefficient depending on pressure, temperature and humidity (simulation WA). The plots are cut at 1 hPa to zoom into the region of interest, although the uppermost model level is at 0.01 hPa. The height values are a logarithmic interpolation from Standard Atmosphere of the pressure array, and the white dotted line shows the climatological tropopause according to Eq. (8).

decreasing by nearly 4 orders of magnitude towards the UTLS. This makes the humidity modification (Eq. 5) most important in the troposphere, where up to 5.5 % of the HO$_2$ + NO reaction form HNO$_3$.

3.1 Effects of the HNO$_3$-forming channel on [HNO$_3$] background

Reaction (R2) is the only major source of HNO$_3$ above about 40 km, putting the relative effect off the scale at altitudes with near zero background [HNO$_3$] (Fig. 1a, 1st row). However, absolute deviations from BA are small there. They have a maximum at 10 hPa, where high absolute HO$_2$ + NO reaction rates meet high HNO$_3$ background mixing ratios. This is an indication for more effective HNO$_3$ loss processes in the altitude range of maximum HNO$_3$ production via (R2).

There is a local [HNO$_3$] increase in the tropical UTLS, due to the maximum of the branching ratio. [HNO$_3$] increases by more than 50 % there in the dry case, confirming the results of Cariolle et al. (2008). The local maximum is even more pronounced when considering humidity. While directly producing HNO$_3$, Reaction (R2) also indirectly reduces the educts for HNO$_3$ formation via NO$_2$ + OH. The latter effect may prevail in the tropical lower troposphere and at an altitude of about 14 km at high latitudes, leading to lower HNO$_3$ mixing rations than in the reference simulation. There is a strong seasonal dependence of the HNO$_3$ response to (R2) (not shown), with reductions at high latitudes only occurring during autumn and spring in the respective hemispheres. Please note that the above discussion refers to [HNO$_3$] calculated online by the chemistry submodel MECCA1, while
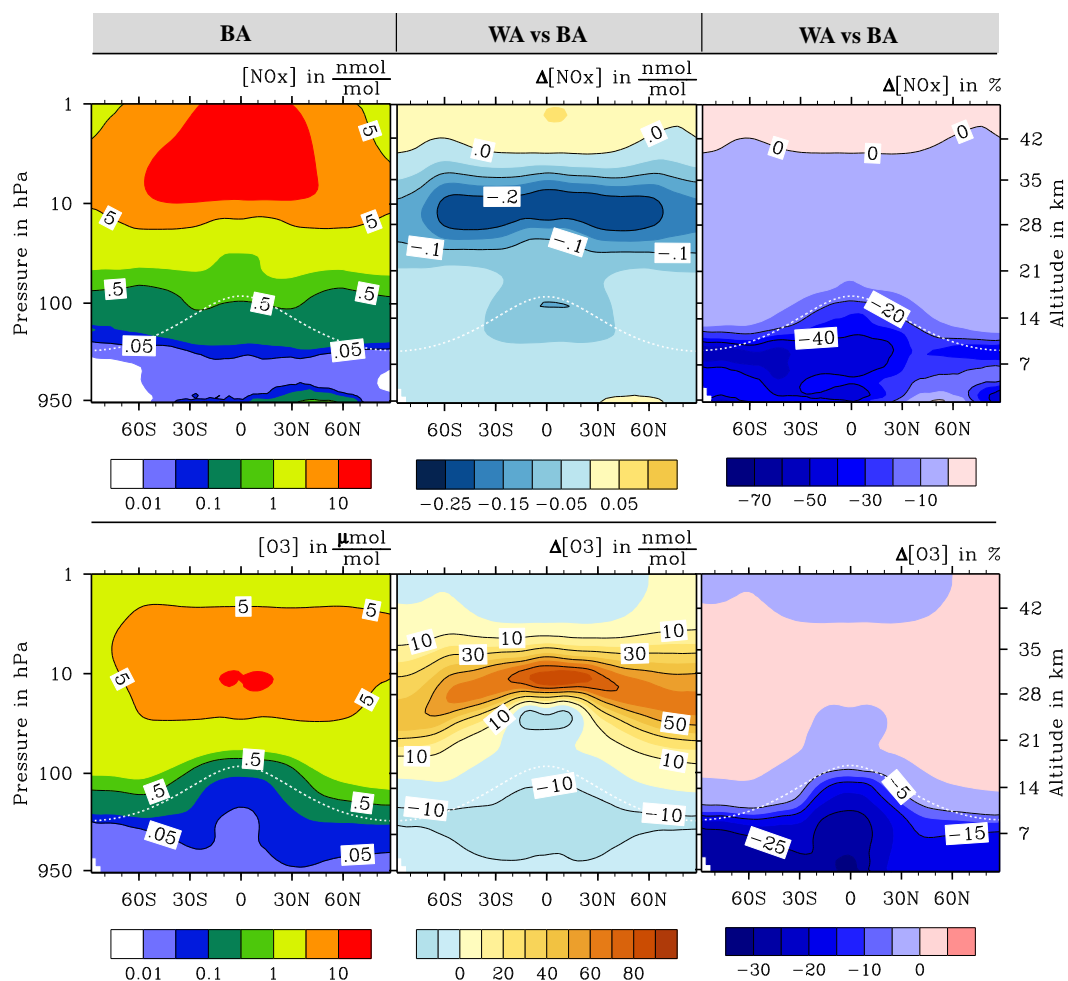
Fig. 1b. As Fig. 1a, but for [NO$_x$] and [O$_3$]. See Fig. S6 of the Supplement for respective plots for [HO$_2$] and [NO$_y$].

all simulations used the same [HNO$_3$] offline climatology for partitioning in polar stratospheric clouds (PSCs). This inconsistency in PSC chemistry must be accepted in order to use the QCTM mode.

3.2 Effects of the HNO$_3$-forming channel on [OH] background

The HNO$_3$ producing channel of HO$_2$ + NO weakens the OH producing channel of this reaction. Therefore [OH] decreases in DA and WA all over, by more than 0.1 pmol mol^{-1} at 10 hPa, across all latitudes (Fig. 1a, 2nd row). This coincides with the maximum absolute impact of Reaction (R2) on [HNO$_3$] and [NO$_x$]. There is a local maximum of absolute [OH] decrease in the tropical UTLS, matching the local maximum of [HNO$_3$] deviations. The local maximum in DA reaches only about 50 % of the corresponding feature in WA. Relative [OH] deviations from BA match those of [NO$_x$]. [OH] decreases by more than 15 % throughout the troposphere in WA. Reaction (R2) shifts the [OH]/[HO]$_2$ ra-

tio towards [HO$_2$] (Supplement, Fig. S7). This effect is most pronounced in the upper troposphere, reaching 29 % in DA and 57 % in WA, both compared to BA.

Following Lawrence et al. (2001), the global OH burden is calculated for the tropospheric domain with a climatological tropopause at

$$p = 300 - 215\,(\cos{(\phi)})^2,\qquad(8)$$

where p is pressure in hPa and ϕ is latitude. The OH concentrations in Table 2 are annual mean values, computed from global monthly mean concentrations $\langle c_{OH}\rangle$:

$$\langle c_{OH}\rangle = \frac{\sum{(w \cdot [OH] \cdot c_{air})}}{\sum{w}},\qquad(9)$$

where $\langle\rangle$ denotes the global spatial integral, the sum $\sum$ is over all grid cells in the tropospheric domain, [OH] is a 3-D field of monthly mean OH mixing ratios, c_{air} is the corresponding 3-D field of the concentration of air (in cm^{-3}), and

Table 2. Global mean hydroxyl radical concentrations (in 10^6 cm^{-3}) and corresponding tropospheric methane lifetimes (τ_{CH_4}, in years) with respect to CH$_4$ + OH $\rightarrow$ CH$_3$ + H$_2$O (Reaction R4). Methane lifetimes for BA, DA and WA are calculated with the recommended reaction rate coefficient for (R4) from Atkinson (2003). The upper boundary is the climatological tropopause defined by Eq. (8). The values of Spivakovsky et al. (2000) are based on observations of CH$_3$CCl$_3$, HCFC-22, and precursors for HO$_x$-NO$_x$ photochemistry.

Reference or simulation	Year(s)	$\langle c_{OH}^{mass} \rangle$	$\langle c_{OH}^{k} \rangle$	$\tau_{CH_4}^{OH}$
Spivakovsky et al. (2000)	1986–1989	1.14	1.32	8.23
Jöckel et al. (2006)	1998–2005	1.08	1.31	8.02
Jöckel et al. (2010)	2001	1.06	1.26	8.54
BA	2001	1.27	1.42	7.6
DA	2001	1.13	1.29	8.4
WA	2001	0.85	0.95	11.4

w is a 3-D field of weighting factors. Weighting with the reaction rate coefficient k_{CH_4} of

$$CH_4 + OH \rightarrow CH_3 + H_2O \qquad (R4)$$

is most relevant to this study, because it determines the methane related radiative forcing terms from aviation NO$_x$. Reaction (R4) is responsible for about 90 % of the global methane breakdown, and accounts for nearly all methane losses in the troposphere (Stenke et al., 2012). Values of the global OH concentration critically depend on the weighting factor and on the domain used for the computation, hampering comparisons between different studies (Lawrence et al., 2001). In order to facilitate comparability, results with grid cell air mass as weighting factor are also provided.

The global OH concentrations ($\langle c_{OH}^{mass} \rangle$, $\langle c_{OH}^{k} \rangle$) of simulation BA are higher than in other modelling studies (Spivakovsky et al., 2000; Jöckel et al., 2006, 2010) that also did not consider (R2). Spivakovsky et al. (2000) utilize a top-down approach, starting from observations of precursors for HO$_x$ -NO$_x$ photochemistry. The global mean OH concentration is then derived from simulations with an accuracy of ± 15 %. BA falls within this uncertainty range. Jöckel et al. (2006) suggest that the differences to Spivakovsky et al. (2000) may lay in the representation of convection (via lightning NO$_x$ and transport of HO$_x$ precursors), or in missing heterogeneous chemical processes. Simulation BA was done with a newer version of EMAC and different emissions, but with an otherwise similar setup as in Jöckel et al. (2006). They prescribed CO emissions of 1097 Tg(CO) yr^{-1}, whereas simulations of the present study had only 862 Tg(CO) yr^{-1}. The difference is mainly in the biomass burning emissions. The reaction CO + OH $\rightarrow$ CO$_2$ + H accounts for approximately 41 % of all tropospheric OH losses (von Kuhlmann et al., 2003). CO emissions in the simulation of Jöckel et al. (2010) ranged from 980 to 1233 Tg(CO) yr^{-1}, for the period 1997 to 2006. Montzka et

al. (2011) show $\langle c_{CO}^{mass} \rangle$ variations of -3.5 % to $+9$ % for that simulation, and $\langle c_{OH}^{mass} \rangle$ is roughly anticorrelated, with $+3$ % to -2.5 %. We have not tested the sensitivity of global [OH] to CO emissions in our model setups, but lower CO mixing ratios might at least partially explain the higher OH levels. An update in the scavenging parameterisation might also have contributed to the differences between EMAC simulations for previous studies (Jöckel et al., 2006, 2010) and the current study (see Appendix B for details).

Reaction (R2) decreases $\langle c_{OH} \rangle$ by about 10 % in DA and by 33 % in WA, both with respect to BA. Are the OH concentrations in DA and WA realistic? Values based on simulations using chemical mechanisms without (R2) may no longer serve as a benchmark here. Direct observations are not suitable for deriving a global climatology or average, due to the short lifetime of OH and spatial variability of [OH]. Indirect estimates of $\langle c_{OH} \rangle$ are based on measurements of longer lived trace gases that are removed from the atmosphere mainly through reactions with OH. Spivakovsky et al. (2000) verify their results with measurements of CH$_3$CCl$_3$, HCFC-22, and others. Global mean OH concentrations derived from the mass balance of these species have an uncertainty of -20 % to $+28$ % with respect to their preferred value (Table 2). BA and DA are within this range, WA is just outside.

Given the general model uncertainties (e.g. emissions), the representation of (R2b) in WA is still covered by observations. For instance, a recent study (Taraborrelli et al., 2012) indicates that a modification of the NMHC oxidation mechanism might increase $\langle c_{OH}^{mass} \rangle$ by 13 %. Considering this, all three simulations would be within the range given by Spivakovsky et al. (2000), i.e. compatible with observations.

3.3 Effects of the HNO$_3$-forming channel on methane lifetime with respect to background [OH]

Methane is a long-lived greenhouse gas, playing an important role in global climate change. Top–down methods for the quantification of methane fluxes are constrained mainly by uncertainties in the sink estimates and the choice of lifetime used in the mass balance calculations (Denman et al., 2007). The lifetime of a gas is essentially its atmospheric mass burden divided by the loss rate. Reaction (R4) mainly determines the lifetime of methane (τ_{CH_4}), which is very sensitive to modifications of OH mixing ratios and distributions. The above uncertainties in [OH] propagate considerable uncertainties on τ_{CH_4} with respect to Reaction (R4) ($\tau_{CH_4}^{OH}$). Recent model based estimates range from $9.72^{+5.33}_{-2.81}$ yr (Shindell et al., 2006), $9.9^{+5.2}_{-3.0}$ yr (Stevenson et al., 2006)[1], or 7.23 to 11.43 yr (Hoor et al., 2009). These values are only comparable to simulation BA, because none of those previous works

---

[1] $\tau_{CH_4}^{OH}$ was not given by Stevenson et al. (2006). The given value is based on their scenario S1, minimum, mean and maximum for all models, a soil sink for methane of 30 Tg yr^{-1}, and a stratospheric sink of 40 Tg yr^{-1}.

considered (R2). Independent estimates of $\tau_{CH_4}^{OH}$ are based on methane and methyl chloroform (MCF = CH$_3$CCl$_3$) observations, giving $9.6_{-1.6}^{+2.4}$ yr (Denman et al., 2007)[2] or 11.2 ± 1.3 yr (Prather et al., 2012). Thus it may serve as a reference for simulations with and without (R2).

Methane lifetime is calculated according to Lawrence et al. (2001), with

$$\tau_{CH_4}^{OH} = \frac{\sum m_{CH_4}}{\langle c_{OH}^k \rangle \cdot \sum \left(k_{CH_4} \cdot m_{CH_4} \right)} \quad (10)$$

for the tropospheric domain defined by Eq. (8). The sums are over all grid boxes in the domain, m_{CH_4} is the methane mass per grid cell, k_{CH_4} is the reaction rate coefficient of (R4), and $\langle c_{OH}^k \rangle$ is the global mean concentration of OH (Eq. 9), weighted by k_{CH_4}. Before calculating the annual mean, Eq. (9) is evaluated with monthly mean 3-D fields of k_{CH_4} and m_{CH_4}, and monthly mean values for $\langle c_{OH}^k \rangle$. About a decade of simulation time would be needed for methane mixing ratios to adjust to a perturbation, while the short-lived [OH] almost immediately adjusts. The actual m_{CH_4} from each simulation enters Eq. (9). However, using methane from BA would reduce $\tau_{CH_4}^{OH}$ in DA and WA by negligible 0.1 yr, compared to the values in Table 2.

Simulation BA is on the low side of estimates for $\tau_{CH_4}^{OH}$ (7.6 yr, Table 2). Methane lifetime increases to 8.4 yr in DA, and to 11.4 yr in WA. All values are in the range of other estimates. Uncertainties in the rate coefficient of (R4) impose uncertainties of up to -30% and $+44\%$ on methane lifetime in the simulations of this study, though the corresponding uncertainties of $\langle c_{OH}^k \rangle$ are small (see Supplement). Methane lifetime changes moderately, if an upper domain boundary of 100 hPa is considered instead of the climatological tropopause (Eq. 8), because (R4) is most important in the troposphere (Stenke et al., 2012). The rate coefficient formulation of Atkinson (2003), as used in this study, is in between the recommendations of IUPAC (2007) and Sander et al. (2011). However, the recommended temperature dependent rate coefficients ($k_{CH_4}^{best}$) of the different studies agree remarkably well (Supplement, Fig. S8).

The methane lifetime change of 10.5% from BA to DA is in good agreement with Søvde et al. (2011), who found 10.9% for a similar comparison with a different model. Cariolle et al. (2008) reported only about 5%. Müller (2011) found $\tau_{CH_4}^{OH} = 7.7$ yr in a simulation without (R2), 8.8 yr when considering (R2) similar to DA, and 9.8 yr for the equivalent to simulation WA. Considering humidity in the rate coefficient of (R2) has a bigger effect in this study. More details about the methodology of Müller (2011) would be needed for an attempt to pinpoint the causes of this difference. Taraborrelli et al. (2012) reported a decrease of methane lifetime from 8.02 yr to 7.2 yr when taking into account OH recycling during NMHC oxidation. Assuming

---

[2] This value follows from a global methane burden of 4929 Tg, and a loss due to (R4) of 511 ± 103 Tg yr^{-1}.

a similar 10% reduction of methane lifetime in simulations BA, DA and WA would bring $\tau_{CH_4}^{OH}$ in WA closest to the observation based value of Denman et al. (2007). WA is the only regime consistent with the MCF-derived $\tau_{CH_4}^{OH}$ of Prather et al. (2012), with and without 10% reduction.

3.4 Effects of the HNO$_3$-forming channel on [NO$_x$] background

As for [HNO$_3$] and [OH], the biggest absolute effects on annual zonal mean [NO$_x$] manifest themselves at about 10 hPa, where [NO$_x$] decreases by up to 251 pmol mol^{-1} in DA and by up to 245 pmol mol^{-1} in WA (Fig. 1b, 1st row). There is an altitude of less [NO$_x$] changes around 70 hPa, followed by a region of again pronounced [NO$_x$] reduction at 100 hPa in the tropics. Humidity effects are bigger there, with the maximum decrease above the equator being 60 pmol mol^{-1} in DA and 100 pmol mol^{-1} in WA. [NO$_x$] is reduced throughout the troposphere, except between 30° N and 70° N, near emission sources at the ground. This indicates a non-monotonic response, depending on NO$_x$ background mixing ratios. There is another region of zero net [NO$_x$] change around 3 hPa, corresponding to the highest NO$_x$ background concentrations.

The relative NO$_x$ effect most pronounced in the troposphere, reaching -35% in DA and -60% in WA. It is skewed towards the less polluted Southern Hemisphere, as noted already by Cariolle et al. (2008).

The response of atmospheric chemistry to aircraft NO$_x$ emissions depends on NO$_x$ background mixing ratios (Ehhalt and Rohrer, 1994). This nonlinear effect will ultimately impact on estimates of radiative forcing due to aviation NO$_x$, independent of the causes for the modified NO$_x$ background.

3.5 Effects of the HNO$_3$-forming channel on [O$_3$] background

As shown in the second row of Fig. 1b, the decrease in NO$_x$ near 10 hPa corresponds to increased ozone mixing ratios in DA and WA. However, the effect of (R2) on [O$_3$] changes sign in this sensitivity block at altitudes of 14 km above the poles and 26 km above the equator. Reaction (R1) produces NO$_2$, and the subsequent photolysis of NO$_2$ is a major source of O$_3$ in the troposphere. NO$_x$ mixing ratios decrease due to Reaction (R2), and the [NO]/[NO$_2$] ratio is additionally shifted towards [NO] (Supplement, Fig. S7). Both effects result in less ozone production via NO$_2$ photolysis. There is a monotonic ozone response to [NO$_x$] perturbations at aircraft flight altitudes and the reduced [NO$_x$] background in DA and WA moves the chemical system away from the nonlinear region. Transport is superimposed on these chemical effects: compared to a simulation without (R2), there is less ozone in the tropical upwellings, and more ozone in the downwellings at high latitudes. Ozone decreases below the altitude of zero net change throughout the troposphere. The relative impact on ozone is most pronounced in the troposphere,
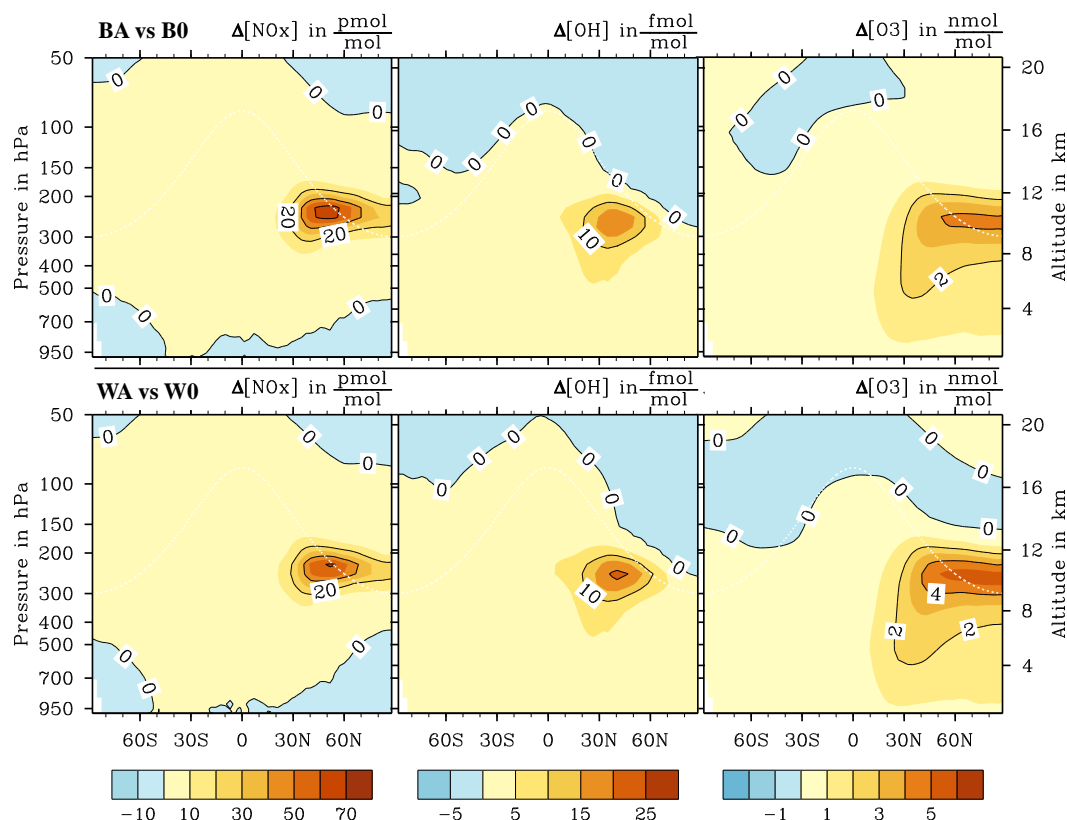
Fig. 2a. Absolute deviations (BA-B0, WA-W0) of annual zonal mean mixing ratios of NO$_x$, OH and O$_3$ in a simulation with aviation NO$_x$ from one without. Simulations without (top), and with HO$_2$ + NO $\rightarrow$ HNO$_3$ assuming a rate coefficient depending on pressure, temperature and humidity (bottom).

where background concentrations are low. It reaches -11% in DA and -32% in WA. There is no big difference between the stratospheric ozone effects in DA and WA. Mixing ratios increase by up to 1.5 % there.

Higher atmospheric density in the troposphere over-compensates higher absolute ozone increases in the strato-sphere. Thus the global annual mean ozone column de-creases, from 316 DU in simulation BA, by 0.5 % in DA, and by 1.8 % in WA (Table 1). A comparison to TOMS total ozone (http://toms.gsfc.nasa.gov/ftpdata_v8.html, not shown) revealed a slight high bias of model O$_3$, as already noted by Jöckel et al. (2006). Compared to their coupled sim-ulations, using a HNO$_3$ climatology for decoupling tends to average out individual PSC events, and impairs denitrifica-tion and ozone destruction further. The effects of (R2) tend to improve the model results.

4   Chemical effects of aviation NO$_x$

In this section the effects of identical aircraft NO$_x$ emissions in three different atmospheric chemical regimes are isolated. The three background regimes are discussed in the previous section. Three different reference cases without aircraft NO$_x$

emissions are introduced (Table 1: B0, D0, W0), one for each regime. Here each sensitivity block refers to a pair of simu-lations within the same chemical regime: ΔB refers to BA versus B0, ΔD to DA versus D0, and ΔW to WA versus W0. This notation applies to absolute (e.g. BA-B0) and relative (e.g. 100{BA-B0}/B0) deviations between the two simula-tions of each pair.

4.1   Chemical effects of aviation NO$_x$ on [NO$_x$]

The plots for aviation effects (Fig. 2a and b) are cut at the 50 hPa level to zoom into the altitude range where aircraft fly. The colour bar does not cover the full range of values in each picture to improve the visibility of the interesting fea-tures. The subsequent discussion refers to annual zonal mean values for the simulation year 2001.

Aircraft NO$_x$ emissions peak in the mid-latitudes of the Northern Hemisphere (NH), between 8 and 12 km altitude. Compared to simulation B0, annual zonal mean [NO$_x$] in-creases in simulation BA by up to 66 pmol mol^{-1} due to air-craft emissions. Reaction (R2) generally decreases [NO$_x$] in the simulations, which also affects NO$_x$ from aviation. Thus [NO$_x$] increases slightly less when Reaction (R2) is included, by up to 64 pmol mol^{-1} in sensitivity block ΔD, and by only
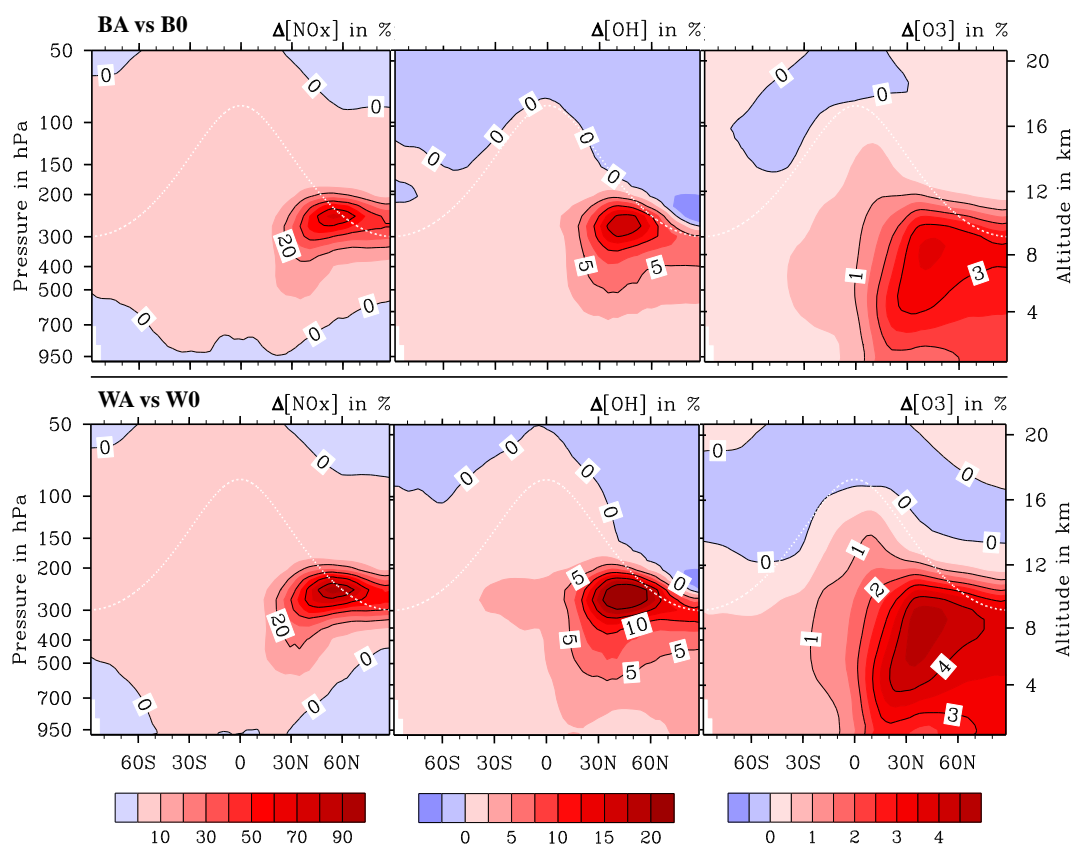
Fig. 2b. As Fig. 2a, but percental deviations relative to the respective simulation without aviation NO$_x$, i.e. $100 \cdot \frac{\text{BA}-\text{B0}}{\text{B0}}$ and $100 \cdot \frac{\text{WA}-\text{W0}}{\text{W0}}$.

61 pmol mol^{-1} in ΔW (Fig. 2a, 1st column). In contrast, the relative effect of aviation NO$_x$ increases when background NO$_x$ is lower due to Reaction (R2) (Fig. 2b, 1st column). It reaches 73 % for sensitivity block ΔB, 83 % for ΔD, and 97 % for ΔW. The lowering effect of (R2) on [NO$_x$] affects the background chemistry more than the perturbation by emissions.

In northern mid-latitudes near the ground, aircraft NO$_x$ emissions decrease NO$_x$ mixing ratios in all sensitivity blocks. This corresponds to the only tropospheric region, where Reaction (R2) increases [NO$_x$] (as discussed in Sect. 3.4).

4.2 Chemical effects of aviation NO$_x$ on [O$_3$]

Ozone mixing ratios in the troposphere rise in response to the additional NO$_x$ from aviation, by up to 4.2 nmol mol^{-1}, 4.7 nmol mol^{-1} and 5.4 nmol mol^{-1} for ΔB, ΔD, and ΔW, respectively (Fig. 2a, 3rd column). The annual mean peak ozone perturbation in sensitivity block ΔB agrees well with those found by other studies: 4.5 nmol mol^{-1} (Fichter, 2009), about 4 nmol mol^{-1} (Grewe et al., 2002), 4.3 nmol mol^{-1} (Gauss et al., 2006), 2.8 nmol mol^{-1} (Hoor et al., 2009), 6 to 9 nmol mol^{-1} (Koehler et al., 2008).

Relative effects on ozone are additionally pronounced when (R2) is considered, because (R2) lowers [O$_3$] in the troposphere. Ozone mixing ratios increase by up to 3.6 % in ΔB, 3.9 % in ΔD, and 4.7 % in ΔW (Fig. 2b, 3rd column). Absolute and relative ozone perturbations are transported further, and are thus not as localized as the shorter lived [NO$_x$] perturbations. There are regions in the stratosphere, where ozone mixing ratios decrease in response to aviation NO$_x$ (Fig. 2a). This is expected from photochemical considerations (Sect. 1), but difficult to interpret here. There are no direct aircraft NO$_x$ emissions from the inventory into the altitude range of negative ozone response. Ozone perturbations in Fig. 2 show the integrated results of photochemistry and the transport of species with different lifetimes. The annual global mean ozone burden increases due to aviation NO$_x$ in all sensitivity blocks, but most in ΔW (Table 1). This is consistent with the known increase in ozone production as [NO$_x$] decreases (Lin et al., 1988; Wu et al., 2009).

4.3 Chemical effects of aviation NO$_x$ on [OH]

Mixing ratios of the hydroxyl radical, [OH], increase in the troposphere in response to aircraft NO$_x$ emissions. The peak perturbation in ΔB is 19 fmol mol^{-1} or 17 %. Additional NO$_x$ in the troposphere enhances (R1), shifting the

Table 3. Global annual mean parameters relevant for radiative forcing calculations. All are evaluated for the region below an upper boundary of 50 hPa. $\Delta\left\langle[O_3]^{\text{short}}\right\rangle$ is the short-lived increase of the ozone burden due to aircraft NO$_x$ emissions, compared to the respective base case. $\left\langle c_{\text{OH}}^k\right\rangle$ is the hydroxyl radical concentration. Methane lifetime ($\tau_{\text{CH}_4}^{\text{OH}}$) is calculated from the [OH] field of the respective simulation, but [CH$_4$] is always from BA. $\left\langle[\text{CH}_4]\right\rangle$ is the methane burden, derived independently for each sensitivity block from monthly mean values of relative methane lifetime change. The same observation based value of $\left\langle[\text{CH}_4]\right\rangle$ is assumed for BA, DA and WA as a reference to calculate a hypothetical methane burden for B0, D0 and W0, respectively.

Simulation	BA	B0	DA	D0	WA	W0
$\Delta\left\langle[O_3]^{\text{short}}\right\rangle$, in DU	0.4933	0	0.5238	0	0.5653	0
$\left\langle c_{\text{OH}}^k\right\rangle$, in 10^6 cm^{-3}	1.41	1.39	1.28	1.26	0.947	0.924
$\tau_{\text{CH}_4}^{\text{OH}}$, in years	8.38	8.49	9.25	9.40	12.49	12.81
$\left\langle[\text{CH}_4]\right\rangle$, in nmol mol^{-1}	1770	1793	1770	1797	1770	1813

[OH]/[HO$_2$] ratio towards [OH] (Supplement, Fig. S7). Furthermore, OH production is increased, due to additional O$_3$ photolysis and the subsequent reaction with water vapour. Note a small spot of decreasing [OH] at high northern latitudes, just above the tropopause. The [OH] response to aviation NO$_x$ changes sign in the same altitude in all sensitivity blocks, regardless of different NO$_x$ and HO$_x$ background mixing ratios. Only the meteorology is identical in all simulations, and there is the same emission perturbation in all sensitivity blocks. Thus pressure- and temperature dependence of reaction rate coefficients in the base photochemical mechanism (i.e. independent of R2) dominate the non-monotonic response of [OH].

Both, absolute and relative effects on [OH] are stronger, when (R2) is considered: peaking at 20 fmol mol^{-1} (20 %) for ΔD, and 21 fmol mol^{-1} (25 %) for ΔW (Fig. 2a and b, 2nd column). Perturbation patterns for the OH concentration, c_{OH}^k, look similar to [OH] perturbations in Fig. 2. Peak values are 0.167×10^6 cm^{-3} (18 %) for ΔB, 0.169×10^6 cm^{-3} (20 %) for ΔD, and 0.173×10^6 cm^{-3} (25 %) for ΔW.

Global annual mean OH concentrations (Eq. 9) for the region below 50 hPa are given in Table 3. About a decade of simulation time would be needed for methane mixing ratios to adjust to a perturbation. The corresponding methane lifetimes are calculated according to Eq. (10, always taking [CH$_4$] from simulation BA. Using the same distribution for all sensitivity blocks is methodologically cleaner for analysing the differences between them, although using other [CH$_4$] would change $\tau_{\text{CH}_4}^{\text{OH}}$ only by ~ 1 %. Methane lifetime in Table 3 is derived from monthly mean values. Aviation NO$_x$ increases $\left\langle c_{\text{OH}}^k\right\rangle$ in ΔD more than in ΔB, but most in ΔW (Table 4). Methane lifetime reduces accordingly, most in ΔW (Table 4).

4.4 Contrasts between aviation NO$_x$ effects for different implementations of the HO$_2$ + NO reaction

Summarizing the chemical effects, aviation NO$_x$ increases [NO$_x$], [OH] and [O$_3$] in all sensitivity blocks. Absolute and relative effects on [OH] and [O$_3$] are more pronounced when considering Reaction (R2), most in sensitivity block ΔW.

Why is (R2) enhancing the effects on [OH] and [O$_3$]? Production and loss of peroxy radicals and ozone depend nonlinearly on temperature, pressure and ambient concentrations of other chemical species (e.g. NO$_x$). Generally, (R2) changes the response function of those production and loss terms to a [NO$_x$] perturbation. In addition the changed chemical background due to (R2) shifts the response depending on ambient concentrations. Both effects change production and loss rates, translating into modified mixing ratios. Differences between sensitivity blocks ΔB, ΔD and ΔW are consequently due directly to the different chemical mechanisms, and indirectly to the resulting different background mixing ratios. More ideas may be found in Sect. 2.4 of the Supplement. The sensitivity method used for this study provides only one final response of [NO$_x$], [OH] and [O$_3$] to a [NO$_x$] perturbation. In order to find the response functions for each sensitivity block, production and loss terms for OH and O$_3$ would have to be evaluated for the relevant atmospheric conditions and for a range of different ambient concentrations. A box modelling approach would be suited for this and might be warranted for a future study, if Reaction (R2) becomes established. Tagging (Grewe et al., 2010) or small perturbation methods (Hoor et al., 2009) might then help to disentangle the different – possibly nonlinear – effects leading to the final response of [NO$_x$], [OH] and [O$_3$].

5 Radiative forcing effects

Four radiative forcing (RF) effects due to aviation NO$_x$ chemical perturbations are considered here: (i) the short-

Table 4. Changes in methane concentration and lifetime, as well as radiative forcing for 0.847 Tg aviation N per year in an atmosphere without Reaction (R2) (ΔB), with (R2a) (ΔD), and (R2b) (ΔW). The other $RF_{O_3}^{short}$ values are based on the stratospheric adjusted RF diagnostic of Dietmüller (2011), i.e. Eq. (11). All other long-lived forcing terms reflect the steady state response of the atmosphere to sustained aircraft NO_x emissions of the year 2000, based on methane lifetime changes due to [OH] perturbations. $RF_{CH_4}^{long}$ and $RF_{O_3}^{long}$ are calculated according to Ramaswamy et al. (2001), $RF_{H_2O}^{long}$ according to Myhre et al. (2007): Eqs. (11), (16), (17) and (18). All results refer to the global domain with an upper boundary at 50 hPa. Uncertainties are discussed in Sect. 5, including those terms without explicitly given error margin.

	ΔB	ΔD	ΔW
$\Delta \left\langle c_{OH}^k \right\rangle$, in %	$+1.51$	$+1.83$	$+2.58$
$\Delta \tau_{CH_4}^{OH}$, in %	$-1.28^{+0.01}_{-0.03}$	$-1.52^{+0.01}_{-0.03}$	$-2.45^{+0.01}_{-0.03}$
$RF_{CH_4}^{long}$, in mW m^{-2}	-11.6 ± 1.1	-13.8 ± 1.2	-22.2 ± 1.8
$RF_{O_3}^{long}$, in mW m^{-2}	-4.1 ± 1.0	-4.8 ± 1.2	-7.8 ± 1.8
$RF_{H_2O}^{long}$, in mW m^{-2}	-2.0 ± 0.5	-2.4 ± 0.6	-3.9 ± 0.9
$RF_{O_3}^{short}$, in mW m^{-2}	$+17.9$	$+19.4$	$+21.8$
net RF, in mW m^{-2}	$+0.2 \pm 2.6$	-1.6 ± 3.0	-12.1 ± 4.6

lived O_3 response as discussed in Sect. 4.2, (ii) the long-lived methane response due to modified [OH] (Sect. 4.3), (iii) a long-lived ozone response due to [CH_4] changes, and (iv) modifications to stratospheric water vapour from methane oxidation. The net RF is the relatively small sum of larger positive (i) and larger negative (ii, iii, iv) components. Like in other studies (Hoor et al., 2009; Myhre et al., 2011), radiative forcing calculations are limited to the chemical perturbations in the altitude range between the surface and 50 hPa. This is within the validity range of the applied rate coefficient parameterisations for (R2) and captures almost all aviation NO_x effects. Tests using the top of the computational domain (0.01 hPa) as upper boundary show that compared to the 50-hPa-top, methane related RFs decrease by less than 3 % and the short-lived ozone forcing by about 0.1 %.

5.1 Radiative forcing from the short-lived ozone response to aviation NO_x

Simulations B0, D0 and W0 are repeated in purely dynamical mode with a modified version of the EMAC radiation module (Dietmüller, 2011, based on Stuber et al., 2001). The radiation module is called twice during the model integration, for the reference case and for the perturbed case. Monthly mean 3-D fields of [O_3] from B0 are provided to the module together with the ozone perturbation ($\Delta B = BA - B0$) due to aviation NO_x. All perturbations above 50 hPa were set

to zero, then using B0 + ΔB to calculate radiation for the perturbed case.

The shortwave radiative forcing is solely determined by the ozone perturbation. The temperature used for dynamics is consistent with [O_3] of the reference case. Longwave radiative fluxes are influenced by temperature, which within the troposphere remains unchanged from the reference to the perturbed radiative flux profile. A second diagnostic temperature field is determined for the perturbed case, which represents the new radiative equilibrium induced by the ozone perturbation in the stratosphere (Hansen et al., 1997; Stuber et al., 2001). These diagnostic temperatures are allowed to adjust to changing [O_3] perturbations constantly. The additional radiative flux change induced by the stratospheric temperature adjustment is counted as an integral part of the longwave ozone radiative forcing.

To calculate RF at the tropopause we need a monthly tropopause climatology, which is derived from BA according to the WMO definition (WMO, 1992) based on the temperature lapse rate for latitudes equatorward of 30°. The climatological value (Eq. 8) was used when no lapse rate was found. At latitudes poleward of 30° the potential vorticity isosurface of 3.5 PVU defined the tropopause. In addition to [O_3], monthly mean climatologies of the radiatively active substances CH_4, N_2O, $CFCl_3$ and CF_2Cl_2 are derived from the year 2001 output of the reference simulations to use the radiation module without online chemistry. Dynamics is nudged for 2000 and 2001, and the first year was discarded for spin-up of the stratospheric temperature adjustment to the perturbed ozone field in the radiation module.

The stratospheric-adjusted radiative forcing from short-lived ozone perturbations is then calculated as the global mean of

$$RF_{O_3}^{short} = \left(\Phi_A^{sw} + \Phi_A^{lw} \right) - \left(\Phi_0^{sw} + \Phi_0^{lw} \right) \quad (11)$$

Φ^{sw} is the net shortwave radiation flux at the tropopause and Φ^{lw} is the longwave flux. Index "A" denotes a simulation with aircraft NO_x emissions (i.e. BA, DA or WA) and index 0 refers to the corresponding reference simulation (B0, D0 or W0). Annual mean values for $RF_{O_3}^{short}$ are listed in Table 4, and monthly mean integrals are shown in Fig. C1 for the three sensitivity blocks (ΔB, ΔD and ΔW). Assuming less interannual than seasonal variability, $RF_{O_3}^{short}$ might not change by more than 10 % from year to year (Appendix C).

Holmes et al. (2011) used a different methodology to estimate $RF_{O_3}^{short}$ for 21 different simulations from recent studies. Scaling their results linearly to the total aircraft NO_x emissions in our simulations, leads to $RF_{O_3}^{short}=18.3 \pm 6.1$ mW m^{-2}. Reaction (R2) was not considered in any of these simulations, and applying Eq. (D1) to sensitivity block ΔB (Appendix D) gives a nearly identical result (18.2 mW m^{-2}). The ozone response to aviation NO_x calculated in ΔB is reasonable for an atmosphere without the HNO_3-forming channel of $HO_2 + NO$.

Equation (D1) illustrates that RF$_{O_3}^{\text{short}}$ is determined essentially by absolute [O$_3$] perturbations. Those are shown in Fig. 2b for sensitivity blocks ΔB and ΔW, and summarized in Table 3 for all sensitivity blocks. Aviation NO$_x$ causes $\langle[O_3]^{\text{short}}\rangle$ to increase least in ΔB and most in ΔW. This is reflected by RF$_{O_3}^{\text{short}}$, which is up to 3.9 mW m^{-2} higher when considering Reaction (R2) (Table 4).

5.2 Methane related radiative forcings

Decadal simulations would be required to reach a steady state response of CH$_4$ to any chemical perturbation, due to the long atmospheric lifetime of methane (Tables 2 and 3). For this study just one year is evaluated per simulation. Furthermore, the setup features prescribed surface mixing ratios for CH$_4$. It does not include CH$_4$ emissions explicitly, inhibiting the attribution of methane changes to chemical perturbations. Thus methane perturbations cannot be quantified from the simulations of this study directly. However, in the troposphere and UTLS methane is almost exclusively affected by Reaction (R4) (Sects. 3.2 and 3.3), governed by

$$\frac{d[CH_4]}{dt} = -[CH_4] \cdot [OH] \cdot k_{CH_4} \tag{12}$$

Methane perturbations due to aircraft NO$_x$ emissions may be estimated from the corresponding [OH] perturbations, which almost immediately adjust due to the short lifetime of OH. Methane effects trail the time of NO$_x$ emission by τ_{CH_4}, and previous emissions determine the actual methane related RF. However, we do not make any assumptions about previous emissions, but analyse the projected steady state response of the atmosphere to sustained aircraft NO$_x$ emissions of the year 2000 instead. Considering the smaller pre-2000 emissions would reduce methane effects by about 30 to 35 % (Grewe and Stenke, 2008; Myhre et al., 2011).

The long lifetime of methane implies that the spatial distribution of [CH$_4$] perturbations is determined by atmospheric mixing, and thus almost independent of the original [OH] perturbation. This would not be captured by translating localized [OH] perturbations (Fig. 2) directly into 3-D methane perturbations. Thus we do not attempt to estimate RF$_{CH_4}^{\text{direct}}$ from 3-D methane fields with radiative transfer calculations, but adopt the approaches of Ramaswamy et al. (2001) and Holmes et al. (2011) that rely on globally integrated quantities for methane perturbations. Note that [OH] perturbations and thus methane related forcings nevertheless critically depend on the location of the original [NO$_x$] perturbation.

Following Ramaswamy et al. (2001):

$$RF_{CH_4}^{\text{direct}} = a\left(\sqrt{M_A} - \sqrt{M_0}\right) \tag{13}$$

$$-b \cdot \ln\left\{\frac{1 + c \cdot (M_A N)^{0.75} + d \cdot M_A \cdot (M_A N)^{1.52}}{1 + c \cdot (M_0 N)^{0.75} + d \cdot M_0 \cdot (M_0 N)^{1.52}}\right\}$$

in Wm^{-2}, with $a = 0.036$, $b = 0.47$, $c = 2.01 \times 10^{-5}$, $d = 5.31 \times 10^{-15}$. The global mean methane mixing ratio at the surface in a simulation with aviation is $M_A = \langle[CH_4]_A\rangle$, in the reference simulation M_0, and $N = \langle[N_2O]\rangle$, all in nmol mol^{-1}. The second term on the right hand side is a correction for the overlap with N$_2$O (Berntsen et al., 2005). Monthly global mean methane mixing ratios for 2001 are estimated from NOAA/GMD data (Forster et al., 2007) by applying a cosine variation of ±7 nmol mol^{-1} to an annual mean value of 1770 nmol mol^{-1}. Those observation based values are assigned to M_A in each sensitivity block (i.e. to BA, DA, WA; Table 3), since observations are affected by aircraft NO$_x$ emissions. Monthly combined nitrous oxide data are from the NOAA/ESRL global monitoring division (HATS_Global_N2O in ftp://ftp.cmdl.noaa.gov/hats/n2o/combined/HATS_global_N2O.txt), giving a mean value of 316.338 nmol mol^{-1} for 2001. Only the global methane mixing ratios for hypothetical atmospheres without aviation are derived from simulations B0, D0 and W0 (Table 3):

$$M_0 = M_A - \Delta\tau_{CH_4}^{\text{OH}} \cdot M_A \tag{14}$$

The relative methane lifetime change,

$$\Delta\tau_{CH_4}^{\text{OH}} = \frac{\left(\tau_{CH_4}^{\text{OH}}\right)_A - \left(\tau_{CH_4}^{\text{OH}}\right)_0}{\left(\tau_{CH_4}^{\text{OH}}\right)_0} \tag{15}$$

is calculated by applying Eq. (10) to monthly mean fields. Methane oxidation (R4) causes [OH] to increase when [CH$_4$] decreases, leading to a further [CH$_4$] loss. This chemical feedback would lead to a different M_0 in a decadal long-term simulation, compared to an estimate based on the initial perturbation. It is thus considered as an additional term of the total long-lived methane RF here, estimated as a fraction of the direct forcing:

$$RF_{CH_4}^{\text{long}} = RF_{CH_4}^{\text{feedback}} + RF_{CH_4}^{\text{direct}} = (1 + f_1) \cdot RF_{CH_4}^{\text{direct}} \tag{16}$$

A feedback factor of $f_1 = 0.4 \pm 0.1$ (Holmes et al., 2011) is used here, which is slightly higher than earlier estimates (Ramaswamy et al., 2001: $f_1 = 0.3 \pm 0.05$). Tropospheric ozone decreases due to the enhanced methane oxidation, caused by aviation NO$_x$. This long-lived ozone effect enhances the methane forcing by another 30 % to 40 % (Ramaswamy et al., 2001), i.e. $f_2 = 0.35 \pm 0.05$:

$$RF_{O_3}^{\text{long}} = f_2 \cdot RF_{CH_4}^{\text{long}} \tag{17}$$

Oxidation of methane is a major source of stratospheric water vapour. The radiative forcing from a water vapour perturbation is estimated to be 15 to 20 % of the direct methane forcing (Myhre et al., 2007), i.e. $f_3 = 0.175 \pm 0.025$:

$$RF_{H_2O}^{\text{long}} = f_3 \cdot RF_{CH_4}^{\text{long}} \tag{18}$$

The results for all forcings in all sensitivity blocks are given in Table 4, together with the relative changes of methane lifetime, the relative perturbation of $\langle c_{OH}^k\rangle$ and the sum of all

RF terms. $RF_{CH_4}^{long}$ is only affected by uncertainties from f_1. The biggest possible uncertainties inherited from the feedback factors f_1 & f_2 and f_1 & f_3 are assumed for $RF_{O_3}^{long}$ and for $RF_{H_2O}^{long}$, respectively. Uncertainties associated with the rate coefficient of (R4) (see Supplement) translate into an additional uncertainty for $\Delta\tau_{CH_4}^{OH}$ and all subsequently derived RFs related to methane. The best estimates are calculated with $k_{CH_4}^{best}$ from Atkinson (2003) and the extremes cover results obtained with $k_{CH_4}^{min}$ or $k_{CH_4}^{max}$ from IUPAC (2007), see Sect. 3 of the Supplement. Seasonal variations of meteorological and chemical situations seem to have little impact on forcings that are due to [OH] perturbations (Appendix C). Interannual variation of the long-lived RF terms is expected to be small.

For comparison, we additionally calculated $RF_{CH_4}^{long}$ and $RF_{O_3}^{long}$ according to the factor decomposition method of Holmes et al. (2011), see Appendix D. The results for sensitivity block ΔB from both methods (Ramaswamy et al., 2001 versus Holmes et al., 2011) agree even better than for $RF_{O_3}^{short}$, indicating little methodological uncertainties.

Note that from all the chemical perturbations in the sensitivity blocks ΔB, ΔD and ΔW, only relative variations of $\tau_{CH_4}^{OH}$ enter Eqs. (16), (17), (18), (D2) and (D3). Consequently the relative response of [OH] to aviation NO$_x$ determines the methane related radiative forcing terms. This is in contrast to $RF_{O_3}^{short}$, which is determined by absolute [O$_3$] perturbations.

Linear scaling of the values based on 21 other simulations from 10 different models (Holmes et al., 2011, factor decomposition method) to 0.847 Tg(N) yr^{-1} leads to $RF_{CH_4}^{long} = -13.3 \pm 3.0$ mW m^{-2} and $RF_{O_3}^{long} = -4.5 \pm 1.9$ mW m^{-2}. Values from sensitivity block ΔB are not as negative, but well within the uncertainty ranges given by Holmes et al. (2011).

5.3 Net radiative forcing from aviation NO$_x$ effects

Net RF from aviation NO$_x$ induced perturbations is the sum from large positive and large negative terms, giving a small net forcing with relatively big uncertainty ranges. The ranges given in this study include only uncertainties inherited from the rate coefficient (k_{CH_4}) for CH$_4$ + OH, and from the factors (f_1, f_2, f_3) applied to estimate radiative forcings that could not be calculated directly. Modifications to f_1, f_2, f_3 or k_{CH_4} would apply to all sensitivity blocks in the same way and shift all RF results in one direction. Thus the net forcing for the three sensitivity blocks (ΔB, ΔD, ΔW) could be $(-2.4, -4.6, -16.7)$ mW m^{-2} at the lower, or $(+2.8, +1.4, -7.5)$ mW m^{-2} at the upper end. According to this analysis, the total radiative forcing from aviation NO$_x$ is near zero for ΔB and decreases to significantly negative values for ΔW. Interannual variations of the different radiative forcing terms are likely to shift net RF in the same direction in all sensitivity blocks (Appendix C), retaining the differences between

the chemical regimes. Net RF would still be negative in ΔW considering 10 % uncertainty of $RF_{O_3}^{short}$.

The result from ΔB, i.e. near zero RF from aviation NO$_x$ when not including (R2), is supported by Holmes et al. (2011). After adjusting their results to our methodology (see Appendix D), their model ensemble leads to a net RF of 1.4 mW m^{-2}, with 10 out of 21 simulations attributing a cooling effect to aviation NO$_x$. Another recent study (Unger, 2011) also found a cooling effect from $RF_{O_3}^{short} + RF_{CH_4}^{long} + RF_{O_3}^{long}$, but also a negligible dependence of $RF_{O_3}^{short}$ on the inclusion of (R2a). Her model yields a remarkably low specific $RF_{O_3}^{short}$ of $0.8 \times 10^{-11} \frac{W}{m^2 \cdot kg(N) \cdot year}$, compared to $2.2 \times 10^{-11} \frac{W}{m^2 \cdot kg(N) \cdot year}$ (Holmes et al., 2011), $2.1 \times 10^{-11} \frac{W}{m^2 \cdot kg(N) \cdot year}$ (sensitivity block ΔB), and $2.3 \times 10^{-11} \frac{W}{m^2 \cdot kg(N) \cdot year}$ (sensitivity block ΔD). Unger (2011) reports a high [NO$_x$] bias in the UT of her simulations. Since the ozone response to a [NO$_x$] perturbation decreases for high [NO$_x$] background values, this might explain low specific $RF_{O_3}^{short}$. Considering the relatively small difference between the short-lived ozone forcing in ΔB and ΔD, the negligible impact of (R2) on $RF_{O_3}^{short}$ found by Unger (2011) might be an artefact of the high [NO$_x$] bias. We are not aware of any aviation study for comparison that included (R2) with a humidity dependent rate coefficient. If our assumptions about $k_{2b}(p, T, c_{H_2O})$ are correct, aircraft NO$_x$ emissions have the potential to cool the Earth. Limitations and uncertainties of this result will be summarized in the next section and should be considered, before attaching any practical importance to it.

6 Summary and conclusions

We discussed the global impact of the HO$_2$ + NO $\rightarrow$ HNO$_3$ Reaction (R2) on atmospheric trace gases, particularly on ozone, methane, and their precursors. Previous modelling studies (Brühl et al., 2007; Cariolle et al., 2008; Søvde et al., 2011; Unger, 2011) applied a rate coefficient $k_{2a}(p, T)$ that depends only on pressure and temperature. The present study additionally considers a humidity modification to the rate coefficient, i.e. $k_{2b}(p, T, c_{H_2O})$. Furthermore, we studied the impact of the reaction on the estimates of aviation NO$_x$-related radiative forcing effects.

While the relative effects of the HNO$_3$-forming channel of the HO$_2$ + NO reaction are pronounced in the UTLS, the absolute effects on [HNO$_3$], [NO$_x$], [OH] and [O$_3$] have their maximum at about 10 hPa. HNO$_3$ mixing ratios mostly increase compared to an atmosphere without Reaction (R2). [NO$_x$] generally decreases from the ground up to 1 hPa. This leads to less ozone in the troposphere, but enhances it in the altitude range of highest atmospheric ozone mixing ratios. The global annual mean ozone column in the simulation with $k_{2a}(p, T)$ decreases by 0.5 % compared to

the simulation without the HNO$_3$-forming channel. Reaction (R2) decreases the oxidizing capacity of the atmosphere, leading to a 10.5 % longer methane lifetime in DA. Our results with $k_{2a}(p, T)$ generally confirm the findings of Cariolle et al. (2008) and Søvde et al. (2011). Humidity enhances the effects of (R2), particularly in the lower troposphere with its high water mixing ratios. The ozone burden decreases by 1.8 % and methane lifetime increases by 50 % when comparing the simulation with $k_{2b}(p, T, c_{H_2O})$ to the simulation without (R2). Methane lifetime is an important parameter for estimating global methane budgets (Denman et al., 2007; Stenke et al., 2012). The uncertainties associated with HO$_2$ + NO → HNO$_3$ propagate a considerable additional uncertainty on methane lifetime estimates that involve modelling of HO$_x$-NO$_x$ chemistry. This implies additional uncertainties for predictions of future methane abundances, for estimates of lifetime changes due to anthropogenic emissions, and for the corresponding radiative forcing.

The simulations discussed in the previous paragraph (BA, WA, DA) include aircraft NO$_x$ emissions. All agree reasonably well with observations, and neither the two regimes with the HNO$_3$-forming channel, nor the one without could be ruled out on that grounds. Since we cannot decide which background chemistry is correct, we cannot entirely rule out that the differences between the aviation NO$_x$ effects in the three regimes are to some degree artefacts of possibly wrong background mixing ratios. The dependence on temperature of the humidity modification to the rate coefficient of (R2), and to a lesser degree on pressure, is still uncertain (LeBras, 2011).

Aviation NO$_x$ primarily leads to more ozone and more hydroxyl radicals in the altitude-latitude region, where most emissions occur. More tropospheric ozone translates into a positive radiative forcing (RF$_{O_3}^{short}$), i.e. warms the Earth. More hydroxyl radicals destroy more methane, resulting in a negative radiative forcing (RF$_{CH_4}^{long}$). Less methane means less stratospheric water vapour from methane oxidation (RF$_{H_2O}^{long}$). A chemical feedback leads to an ozone decrease in response to less methane, and thus to an additional negative forcing (RF$_{O_3}^{long}$). Whereas RF$_{O_3}^{short}$ acts on the timescale of months, these methane-related radiative forcings act on a timescale of decades. Correcting for different emissions, all forcing terms from the sensitivity block without Reaction (R2) agree very well with the results from a recent multi-model aviation study (Holmes et al., 2011), which did not include (R2). Positive and negative forcings nearly compensate each other for sustained aircraft NO$_x$ emissions of the year 2000, leaving a positive net RF of about +0.2 mW m^{-2} in our study.

Considering HO$_2$ + NO → HNO$_3$ decreases the [NO$_x$] background and increases the effects of aircraft NO$_x$ emissions on [O$_3$] and [OH]. RF$_{O_3}^{short}$ is primarily determined by the absolute ozone perturbation due to aviation NO$_x$. Essentially the same absolute [NO$_x$] perturbation increases [O$_3$] more in the regimes with (R2) than in the one without. This

is consistent with the nonlinear effect of higher ozone production at lower [NO$_x$] background (Lin et al., 1988; Wu et al., 2009). The long lived methane-related forcings RF$_{CH_4}^{long}$, RF$_{O_3}^{long}$ and RF$_{H_2O}^{long}$ are determined by relative methane lifetime changes, and thus by the relative perturbations of OH concentrations. Lower background [OH] due to (R2) directly results in enhanced radiative forcing, even for the same absolute [OH] perturbation. However, [OH] increases more in response to aircraft [NO$_x$] emissions, when the HNO$_3$ forming channel is considered, thus additionally pronouncing RF$_{CH_4}^{long}$, RF$_{O_3}^{long}$ and RF$_{H_2O}^{long}$. All in all the negative forcings are more sensitive to the introduction of HO$_2$ + NO → HNO$_3$ than the positive short-lived ozone forcing, shifting the net forcing related to aviation NO$_x$ towards cooling. The absolute value of net RF depends on various assumptions, e.g. the emission history, the emission inventory, the inclusion of secondary effects from methane perturbations, the methods for gauging chemical perturbations, the methods for estimating radiative forcing for given chemical perturbations, and the chemical background provided by the model. Net aviation NO$_x$ RF decreases for our methodology with sustained emissions to −1.6 mW m^{-2} in the regime with $k_2(p, T)$, and to −12.1 mW m^{-2} in the one with $k_2(p, T, c_{H_2O})$.

Considering the regime with $k_2(p, T, c_{H_2O})$ to be the most likely one, according to the present study, aircraft NO$_x$ emissions are likely to cool the Earth. This tentative conclusion has potentially important implications for strategies, which aim to mitigate aviation RF by NO$_x$ reduction or even trade less NO$_x$ against more CO$_2$ emissions. We note three effects that might be interesting for strategies, which aim to mitigate aviation RF by changing the emission location: (i) most aircraft NO$_x$ emissions occur in the UTLS of NH mid-latitudes, while (R2) impacts most in the tropical UTLS. Emitting more NO$_x$ in latitude-altitude regions where (R2) is more/less important would likely increase/decrease the effects on [O$_3$] and [OH], thereby changing the net forcing. (ii) The current aircraft fleet flies close to the altitude where the [OH] response to NO$_x$ emissions changes sign. Flying only a little bit higher might drastically reduce OH-induced cooling RF effects. (iii) RF$_{O_3}^{short}$ is concentrated in NH mid-latitudes and perturbations take full effect within weeks, while the methane related forcings act globally on a decadal time scale. The time lag between RF$_{O_3}^{short}$ and methane effects also implies that the short-lived positive forcing becomes more important for increasing aircraft NO$_x$ emissions, while the long-lived negative forcings would dominate for decreasing emissions.

However, further research is necessary before any recommendation regarding aircraft NO$_x$ emission reduction can be made. Considering the NMHC oxidation mechanism of Taraborrelli et al. (2012) might increase the [OH] background, reducing the magnitude of methane related RF components in all regimes. Some NO$_x$ related effects are neglected in this study, e.g. formation of nitrate aerosols

(Forster et al., 2007), direct RF from NO$_2$ (Kvalevåg and Myhre, 2007), interaction of O$_3$ and OH perturbations with the sulphate burden (Unger et al., 2006). We also did not consider plume effects in this study, which might reduce the ozone response to aviation NO$_x$ by 10 to 25 % (Cariolle et al., 2009). Furthermore the robustness of our results should be tested with different models and methodologies, e.g. with a small perturbation approach like in Hoor et al. (2009). Above all, further experimental work is urgently needed to consolidate parameterizations of the rate coefficient. This need includes stratospheric conditions, and measurements of the effects of humidity on Reaction (R2) at more than a single configuration of pressure and temperature. The uncertainties associated with the HNO$_3$-forming channel of the HO$_2$ + NO reaction propagate a considerable additional uncertainty on estimates of the radiative forcing due to aircraft NO$_x$ emissions.

Appendix A

QCTM mode

This study focuses on chemical effects, but not on the potential feedbacks between perturbed chemistry and dynamics. Small chemical differences cause a divergence of model dynamics in a coupled system. In such cases, the strategy to compare a base simulation with a chemically modified sensitivity simulation would require very long integration times to find a statistically significant chemical signal, due to the dynamically induced "noise". For small perturbations this might not be possible at all. Therefore EMAC was operated in Quasi Chemistry Transport Model (QCTM) mode (Deckert et al., 2011) for all simulations, switching off any feedback from chemical perturbations to the dynamical state (meteorology) of the atmosphere. The same dynamics is recalculated for each simulation, which – for the chemical calculations – is identical to driving a suite of CTM simulations with the same offline dynamics. The dynamics generated by EMAC is per se not better or worse than dynamics from any other model that could be used to drive a CTM.

The model configuration used here is largely similar to the one used for Deckert et al. (2011). The same predefined climatologies (for radiatively active gases, nitric acid and chemical water vapour tendencies) are used in all simulations to calculate chemical feedbacks on model dynamics. In turn, the meteorological parameters (e.g. temperature, pressure, flow field, radiation, humidity) entering atmospheric chemistry calculations are also identical throughout the suite of simulations. The sensitivity simulations contain only the chemical effects of the applied perturbations. Statistical analyses to extract a chemical signal are therefore not necessary. Model meteorology and emissions in the simulations do both depend on time though. However, a statistical evaluation of interannual variability of the chemical signal is not possible

for one simulation year. At the most, variation throughout the year may give some indication of the sensitivity of the chemical signal to different states of the background atmosphere.

The analysis of chemical signals from QCTM simulations neglects any potential differences that might occur in response to the feedbacks from chemical perturbations on dynamics, and back from dynamics on atmospheric chemistry. However, aviation induced chemical perturbations are too small to modify meteorology enough to change the chemistry response (Grewe et al., 2002).

Appendix B

Additional model configuration details

An aerosol climatology (Tanre et al., 1984) is used for the calculation of the radiation field and other climatologies (troposphere: Kerkweg (2005), stratosphere: H$_2$SO$_4$ from Stratospheric Aerosol and Gas Experiment – SAGE) to provide aerosol surfaces for heterogeneous chemistry. The chemical setup considered 13 heterogeneous reactions, some of them on different surface types: 11 on nitric-acid trihydrate particles, 11 on polar stratospheric ice clouds, 8 on liquid stratospheric aerosol, and one on liquid tropospheric sulphate aerosol.

The scavenging submodel accounted for 41 aqueous reactions in rain and Langmuir uptake of nitric acid on ice. The code was modified with respect to the standard EMAC version 1.10 to avoid unrealistically high convective liquid and ice water contents[3]. Compared to Tost et al. (2010), this particularly reduced uptake and subsequent removal of nitric acid in the tropical UTLS.

The following emissions from natural and anthropogenic sources are provided to the model as monthly mean offline fields, representing conditions of the simulated period around the year 2000. Transient biomass burning data stem from GFED 3.1 (van der Werf et al., 2010). Anthropogenic non-traffic emissions are taken from the inventory by Lamarque et al. (2010) in support of IPCC 5th Assessment Report. Shipping emissions are based on the same dataset, but are rescaled to the time period 1998–2007 using the scaling factors of Eyring et al. (2010). Road traffic and aircraft emissions for the year 2000 are taken from the QUANTIFY project (Lee et al., 2005; QUANTIFY, 2008). Other sources included NH$_3$ emissions from the EDGAR3.2FT database (van Aardenne et al., 2005), SO$_2$ volcanic emissions from AeroCom (Dentener et al., 2006), terrestrial DMS (Spiro et al., 1992) and biogenic emissions (Ganzeveld et al., 2006). Speciation of Non-Methane Hydro Carbons (NMHCs) is realized following von Kuhlmann et al. (2001), as described also in Hoor et al. (2009).

---

[3] That update has been officially included from EMAC version 2.42 onwards.

Table B1. Applied processes and respective submodels of EMAC.

Submodel	Process	Ref.
AIRSEA	Air-sea exchange	Pozzer et al. (2006)
CLOUD	Large-scale condensation	see Lohmann and Roeckner (1996), Roeckner et al. (2003)
CONVECT	Convection	Tost et al. (2006b)
CVTRANS	Convective tracer transport	see Jöckel et al. (2006)
DRYDEP, SEDI	Dry deposition, aerosol sedimentation	Kerkweg et al. (2006a)
H$_2$O	Stratospheric H$_2$O and feedback	see Jöckel et al. (2006)
HETCHEM	Heterogeneous reaction rates	see Jöckel et al. (2006)
JVAL	Photolysis rate calculations	see Jöckel et al. (2006)
LNOX	Lightning NO$_x$ emissions	Grewe et al. (2001), Tost et al. (2007)
MECCA1	Gas phase chemistry	Sander et al. (2005)
OFFLEM, ONLEM	Emissions	Kerkweg et al. (2006b)
NCREGRID	Automatic grid transformations	Jöckel (2006)
PSC	Partitioning (H$_2$O, HNO$_3$) in PSCs	Kirner et al. (2011)
QBO	QBO nudging	Jöckel et al. (2006)
RAD4ALL	Radiation	see Jöckel et al. (2006)
SCAV	Scavenging, aqueous phase chemistry	Tost et al. (2006a, 2007)
TNUDGE	Tracer boundary conditions	Kerkweg et al. (2006b)
TRACER, PTRAC	Prognostic tracers	Jöckel et al. (2008)
TROPOP	Tropopause diagnostics	Jöckel et al. (2006)

Online emissions of soil NO and isoprene are simulated as a function of specific meteorological conditions. Lightning NO$_x$ production is parameterized following the scheme by Grewe et al. (2001), resulting in 5.5 Tg(N) yr^{-1} in all simulations of this study for the year 2001. This value is close to the observation-based estimate of 5 Tg(N) yr^{-1} (Schumann and Huntrieser, 2007). Boundary conditions for long-lived species (CO$_2$, CH$_4$, N$_2$O, CFCs, HCFCs, Halons and H$_2$) are nudged to prescribed surface mixing ratios as in Jöckel et al. (2006). Finally, external fields for oceanic DMS, isoprene and ocean salinity are provided in order to simulate the exchange between ocean and atmosphere.

All simulations shown were performed on the IBM Power6 system "Blizzard" at Deutsches Klimarechenzentrum (DKRZ Hamburg), using 4 nodes with 64 tasks each, a Rosenbrock-3 solver with the chemistry submodel MECCA1, 12 min model time step, and 5-hourly output. It took about 4.5 h real time to calculate one model month per simulation. This high computational cost was the reason for limiting the simulation period to 24 months.

Appendix C

Monthly variation of radiative forcing

The simulations of this study are evaluated for only one year, prohibiting a direct statistical analysis of interannual variability of the radiative forcing terms. Here RF variation throughout the year is evaluated to give some indication of the sensitivity of the chemical signal to different states of the background atmosphere. This may serve as a proxy for possible interannual variability.

Global monthly mean values of RF$_{O_3}^{short}$ deviate by about -16% to $+13\%$ from the annual mean values (Table 4) in all sensitivity blocks (Fig. C1). This is partly due to the monthly variation of aircraft emissions in the inventory. Those range from 7.16 Gg(NO$_2$) day^{-1} in January to 7.97 Tg(NO$_2$) day^{-1} in September, which is -5% and $+4\%$ with respect to the annual mean of 7.61 Tg(NO$_2$) day^{-1}. Scaling monthly RF values with the respective emissions leaves a variation from -11% to $+9\%$ with respect to the annual mean. This includes any nonlinear dependence of RF on the amount of aircraft emissions, as well as the effects of seasonal weather changes on RF. Assuming less interannual than seasonal variability, RF$_{O_3}^{short}$ might not change by more than 10% from year to year. Note that [NO$_x$] perturbations are reflected in RF$_{O_3}^{short}$ with a delay of about 10 days (lifetime of NO$_x$ in the UTLS).

Perturbations of [OH] affect methane and thus the above RF terms with a delay of about decade (τ_{CH_4}). RF$_{CH_4}^{long}$, RF$_{H_2O}^{long}$ and RF$_{O_3}^{long}$ in Fig. C1 reflect the variations of c_{OH}^k, $\langle[CH_4]_A\rangle$ and $\langle[N_2O]\rangle$ throughout the year, expressed as radiative forcing. However, the actual radiative forcing from any [NO$_x$] perturbation would be smeared over years. There is little variation of RF$_{CH_4}^{long}$, RF$_{H_2O}^{long}$ and RF$_{O_3}^{long}$ throughout the year. Seasonal variations of meteorological and chemical situations seem to have little impact on forcings that are due to [OH] perturbations. Interannual variation for the long-lived RF components is expected to be small.
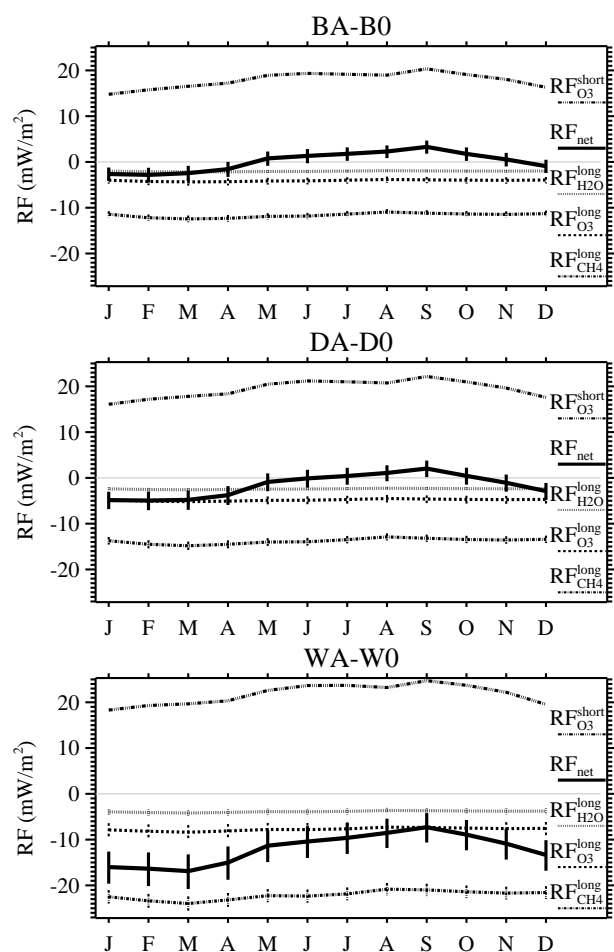
Fig. C1. Monthly mean radiative forcing terms according to Eqs. (11) (Dietmüller, 2011), (16), (17) (Ramaswamy et al., 2001), and (19) (Myhre et al., 2007). Note that RF$_{CH_4}^{long}$, RF$_{H2O}^{long}$ and RF$_{O_3}^{long}$ reflect the almost instantaneous response of [OH] to the [NO$_x$] and [O$_3$] perturbations here, but the actual radiative forcing would rather be determined by the long-term methane response and the seasonal variation of methane mixing ratios. RF$_{O_3}^{short}$ is the actual RF at the time, but aircraft NO$_x$ emissions are not immediately reflected by an ozone perturbation. The error bars are discussed in Appendix C and in Sect. 5.

Appendix D

Radiative forcing according to Holmes et al. (2011)

We also applied the methodology of Holmes et al. (2011) to estimate the radiative forcing for sensitivity blocks ΔB, ΔD and ΔW. This allows us to check the RF results from Sect. 5 with a different methodology, and additionally to compare the RF results from our sensitivity block ΔB to the results from the 21 simulations evaluated by Holmes et al. (2011).

Holmes et al. (2011) derive uncertainty ranges of more than 30 % from an ensemble of simulations, which characterise inter-model uncertainty, but do not apply to our single-

Table D1. Radiative forcing (in mW m^{-2}) for aviation NO$_x$ emissions of 0.847 Tg(N) yr^{-1} in an atmosphere without Reaction (R2) (ΔB), with (R2a) (ΔD), and with (R2b) (ΔW). Values are obtained with the factor decomposition method of Holmes et al. (2011), i.e. Eqs. (D1), (19), (20) and (21). All results refer to the global domain with an upper boundary at 50 hPa. Column "Holmes FD" refers to the results obtained by Holmes et al. (2011) with the factor decomposition method for 21 recent simulations, all without (R2). Column "Holmes ME" refers to the model ensemble method of the same study. All results of Holmes et al. (2011) are linearly scaled to our emissions. Holmes et al. (2011) did not consider RF$_{H_2O}^{long}$.

	Holmes FD	Holmes ME	ΔB	ΔD	ΔW
RF$_{CH_4}^{long}$	-13.3 ± 3.0	-13.6 ± 4.7	-11.9	-14.1	-22.6
RF$_{O_3}^{long}$	-4.5 ± 1.9	-5.6 ± 2.8	-4.0	-4.8	-7.7
RF$_{O_3}^{short}$	$+18.3 \pm 6.1$	$+23.1 \pm 8.2$	$+18.2$	$+19.3$	$+20.8$
net RF without RF$_{H_2O}^{long}$	$+0.5 \pm 7.0$	3.8 ± 3.8	$+2.3$	$+0.5$	-9.5
RF$_{H_2O}^{long}$	-2.3	-2.4	-2.1	-2.5	-4.0

model study. Only the first term of their equation

$$RF_{O_3}^{short} = \frac{\Delta \langle [O_3]^{short} \rangle}{\Delta E} \cdot \frac{dF}{d \langle [O_3] \rangle} \tag{D1}$$

is extracted from our simulations. $\Delta \langle [O_3]^{short} \rangle = \langle [O_3]_A^{short} \rangle - \langle [O_3]_0^{short} \rangle$ is the change of the global mean short-lived ozone burden (in Dobson units) due to aviation NO$_x$ emissions. It is calculated from monthly mean ozone fields. The term $\Delta E = 0.8473$ Tg(N) yr^{-1} is equal to the total aviation NO$_x$ emissions of the QUANTIFY (2008) inventory (Lee et al., 2005), as they are switched off completely in the control simulations B0, D0 and W0. RF$_{O_3}^{short}$ depends on the spatial distribution of the ozone perturbation and on the method to determine RF. Both are hidden in the pre-calculated RF efficiency of tropospheric ozone ($dF/d \langle [O_3] \rangle$). Holmes et al. (2011) adopt the value of Myhre et al. (2011), who also used the QUANTIFY (2008) aviation NO$_x$ inventory (Lee et al., 2005) and stratospheric-adjusted RF, but not the EMAC model.

Applying both methods to our simulations, the corresponding results for RF$_{O_3}^{short}$ agree remarkably well, within 5 % of each other. Note that RF$_{O_3}^{short}$ from both methods agrees least well in sensitivity block ΔW, where the ozone perturbation is expected to differ most from the ones considered by Holmes et al. (2011). Furthermore, modifications of background ozone due to (R2) also affect the radiation available for interacting with the aviation perturbation. In contrast, the direct calculation of RF$_{O_3}^{short}$ captures such deviations and tends to provide a more accurate result here.

For comparison, we additionally calculated $RF_{CH_4}^{long}$ and $RF_{O_3}^{long}$ according to Holmes et al. (2011):

$$RF_{CH_4}^{long} = \frac{\Delta\tau_{CH_4}^{OH}}{\Delta E} \cdot f_1 \cdot M_A \cdot \frac{dF}{d\langle[CH_4]\rangle} \quad (D2)$$

$$RF_{O_3}^{long} = \frac{\Delta\tau_{CH_4}^{OH}}{\Delta E} \cdot f_1 \cdot M_A \cdot \frac{d\langle[O_3]\rangle}{d\langle[CH_4]\rangle} \cdot \frac{dF}{d\langle[O_3]\rangle} \quad (D3)$$

Holmes et al. (2011) excluded stratospheric water vapour from their analysis and $RF_{CH_4}^{long}$ is calculated according to Eq. (18), based on the results from Eq. (D2). Only the relative change of methane lifetime and the aircraft emissions are derived from our simulations. The pre-calculated RF efficiency of tropospheric methane ($dF/d\langle[CH_4]\rangle$) and the coupling term $d\langle[O_3]\rangle/d\langle[CH_4]\rangle$ are adopted from Holmes et al. (2011). The results are given in Table D1, but no uncertainty analysis is attempted.

In addition to applying the methodology of Holmes et al. (2011) to our simulations, we also compare the RF results from the 21 simulations evaluated by the same study to the RF obtained with our model. None of the models evaluated by Holmes et al. (2011) considered the reaction $HO_2 + NO \rightarrow HNO_3$, and thus a fair comparison is only possible to sensitivity block ΔB. We linearly scaled their results to the aircraft NO_x emissions used here, and additionally estimated $RF_{H_2O}^{long}$ according to Eq. (18) from their $RF_{CH_4}^{long}$. The latter is done separately for the individual models and the factor decomposition approach. Then their model ensemble leads to a net RF of $1.4\,mW\,m^{-2}$, with 10 models attributing a cooling effect to aviation NO_x. Without $RF_{H_2O}^{long}$ only 3 models would diagnose a negative net RF. The factor decomposition method shifts their results towards lower forcings (see Table D1). Without considering $RF_{H_2O}^{long}$, 10 out of their 21 simulations yield a negative net RF, which increases to 14 models when accounting for $RF_{H_2O}^{long}$.

All RF results, i.e. ΔB with methodology of Sect. 5, ΔB with factor decomposition method, models of Holmes et al. (2011) with factor decomposition method, and models of Holmes et al. (2011) with ensemble method agree within the given uncertainty ranges.

Supplementary material related to this article is available online at: http://www.atmos-chem-phys.net/13/3003/2013/acp-13-3003-2013-supplement.pdf.

References

Adams, D.: The Hitchhiker's Guide to the Galaxy, Pan Books Ltd., London, United Kingdom, 1979.

Atkinson, R.: Kinetics of the gas-phase reactions of OH radicals with alkanes and cycloalkanes, Atmos. Chem. Phys., 3, 2233–2307, doi:10.5194/acp-3-2233-2003, 2003.

Atkinson, R., Baulch, D. L., Cox, R. A., Crowley, J. N., Hampson, R. F., Hynes, R. G., Jenkin, M. E., Rossi, M. J., and Troe, J.: Evaluated kinetic and photochemical data for atmospheric chemistry: Volume I – gas phase reactions of O_x, HO_x, NO_x and SO_x species, Atmos. Chem. Phys., 4, 1461–1738, doi:10.5194/acp-4-1461-2004, 2004.

Berntsen, T. K., Fuglestvedt, J. S., Joshi, M. M., Shine, K. P., Stuber, N., Ponater, M., Sausen, R., Hauglustaine, D. A., and Li, L.: Response of climate to regional emissions of ozone precursors: sensitivities and warming potentials, Tellus, 57B, 283–304, 2005.

Bohn, B. and Zetzsch, C. J.: Rate Constants of HO2 + NO Covering Atmospheric Conditions. 1. HO_2 Formed by OH + H_2O_2, J. Phys. Chem. A, 101, 1488–1493, 1997.

Brühl, C., Steil, B., Stiller, G., Funke, B., and Jöckel, P.: Nitrogen compounds and ozone in the stratosphere: comparison of MIPAS satellite data with the chemistry climate model ECHAM5/MESSy1, Atmos. Chem. Phys., 7, 5585–5598, doi:10.5194/acp-7-5585-2007, 2007.

Butkovskaya, N., Kukui, A., Pouvesle, N., and Le Bras, G.: Formation of Nitric Acid in the Gas-Phase HO_2 + NO Reaction: Effects of Temperature and Water Vapor, J. Phys. Chem. A, 109, 6509–6520, doi:10.1021/jp051534v, 2005.

Butkovskaya, N., Kukui, A., and Le Bras, G.: HNO_3 Forming Channel of the HO_2 + NO Reaction as a Function of Pressure and Temperature in the Ranges of 72–600 Torr and 223–323 K, J. Phys. Chem. A, 111, 9047–9053, doi:10.1021/jp074117m, 2007.

Butkovskaya, N., Rayez, M.-T., Kukui, A., and Le Bras, G.: Water Vapor Effect on the HNO_3 Yield in the HO_2 + NO Reaction: Experimental and Theoretical Evidence, J. Phys. Chem. A, 113, 11327–11342, doi:10.1021/jp811428p, 2009.

Cariolle, D., Evans, M. J., Chipperfield, M. P., Butkovskaya, N., Kukui, A., and Le Bras, G.: Impact of the new HNO_3-forming channel of the HO_2+NO reaction on tropospheric HNO_3, NO_x, HO_x and ozone, Atmos. Chem. Phys., 8, 4061–4068, doi:10.5194/acp-8-4061-2008, 2008.

Cariolle, D., Caro, D., Paoli, R., Hauglustaine, D. A., Cuénot, B., Cozic, A., and Paugam, R.: Parameterization of plume

chemistry into large-scale atmospheric models: Application to aircraft NO$_x$ emissions, J. Geophys. Res., 114, D19302, doi:10.1029/2009JD011873, 2009.

Chen, C., Shepler, B. C., Braams, B. J., and Bowman, J. M.: Quasiclassical trajectory calculations of the HO$_2$+ NO reaction on a global potential energy surface, Phys. Chem. Chem. Phys., 11, 4722–4727, doi:10.1039/b823031e, 2009.

Deckert, R., Jöckel, P., Grewe, V., Gottschaldt, K.-D., and Hoor, P.: A quasi chemistry-transport model mode for EMAC, Geosci. Model Dev., 4, 195–206, doi:10.5194/gmd-4-195-2011, 2011.

Denman, K. L., Brasseur, G., Chidthaisong, A., Ciais, P., Cox, P. M., Dickinson, R. E., Hauglustaine, D., Heinze, C., Holland, E., Jacob, D., Lohmann, U., Ramachandran, S., da Silva Dias, P. L., Wofsy, S. C., and Zhang, X.: Couplings Between Changes in the Climate System and Biogeochemistry, in: Climate Change 2007: The Physical Science Basis. Contribution of Working Group I to the Fourth Assessment Report of the Intergovernmental Panel on Climate Change, edited by: Solomon, S., Qin, D., Manning, M., Chen, Z., Marquis, M., Averyt, K. B., Tignor, M., and Miller, H. L., Cambridge University Press, Cambridge, United Kingdom and New York, NY, USA, 2007.

Dentener, F., Kinne, S., Bond, T., Boucher, O., Cofala, J., Generoso, S., Ginoux, P., Gong, S., Hoelzemann, J. J., Ito, A., Marelli, L., Penner, J. E., Putaud, J.-P., Textor, C., Schulz, M., van der Werf, G. R., and Wilson, J.: Emissions of primary aerosol and precursor gases in the years 2000 and 1750 prescribed data-sets for AeroCom, Atmos. Chem. Phys., 6, 4321–4344, doi:10.5194/acp-6-4321-2006, 2006.

Dietmüller, S.: Relative Bedeutung chemischer und physikalischer Rückkopplungen in Klimasensitivitätsstudien mit dem Klima-Chemie-Modellsystem EMAC/MLO, Forschungsbericht 2011-19, Deutsches Zentrum für Luft- und Raumfahrt, Germany, 2011.

Ehhalt, D. and Rohrer, F.: The impact of commercial aircraft on tropospheric ozone, Proceedings of the 7th BOC Priestly conference, Lewisburg, Pennsylvania, USA, 1994.

Ehhalt, D., Prather, M., Dentener, F., Derwent, R., Dlugokencky, E., Holland, E., Isaksen, I., Katima, J., Kirchhoff, V., Matson, P., Midgley, P., and Wang, M.: Atmospheric Chemistry and Greenhouse Gases, in: Climate Change 2001: The Scientific Basis. Contribution of Working Group I to the Third Assessment Report of the Intergovernmental Panel on Climate Change, edited by: Houghton, J. T., Ding, Y., Griggs, D. J., Noguer, M., van der Linden, P. J., Dai, X., Maskell, K., and Johnson, C. A., Cambridge University Press, Cambridge, United Kingdom and New York, NY, USA, 239–287, 2001.

Emmons, L. K., Hauglustaine, D. A., Müller, J.-F., Carroll, M. A., Brasseur, G. P., Brunner, D., Staehelin, J., Thouret, V., and Marenco, A.: Data composites of airborne observation of tropospheric ozone and its precursor, J. Geophys. Res., 105, 20497–20538, 2000.

Eyring, V., Isaksen, I. S. A., Berntsen, T., Collins, W. J., Corbett, J. J., Endresen, O., Grainger, R. G., Moldanova, J., Schlager, H., and Stevenson, D. S.: Transport impacts on atmosphere and climate: Shipping, Atmos. Environ., 44, 4735–4771, doi:10.1016/j.atmosenv.2009.04.059, 2010.

Fahey, D. W., Kawa, S. R., Woodbridge, E. L., Tin, P., Wilson, J. C., Jonsson, H. H., Dye, J. E., Baumgardner, D., Borrmann, S., Toohey, D. W., Avallone, L. M., Proffitt, M. H., Margitan, J., Loewenstein, M., Podolske, J. R., Salawitch, R. J., Wofsy, S.

C., Ko, M. K. W., Anderson, D. E., Schoeber, M. R., and Chan, K. R.: In situ measurements constraining the role of sulphate aerosols in mid-latitude ozone depletion, Nature, 363, 509–514, doi:10.1038/363509a0, 1993.

Fichter, C.: Climate impact of air traffic emissions in dependency of the emission location and altitude, Forschungsbericht 2009-22, Deutsches Zentrum für Luft- und Raumfahrt, Germany, 2009.

Forster, P., Ramaswamy, V., Artaxo, P., Berntsen, T., Betts, R., Fahey, D. W., Haywood, J., Lean, J., Lowe, D. C., Myhre, G., Nganga, J., Prinn, R., Raga, G., Schulz, M., and Van Dorland, R.: Changes in Atmospheric Constituents and in Radiative Forcing, in: Climate Change 2007: The Physical Science Basis. Contribution of Working Group I to the Fourth Assessment Report of the Intergovernmental Panel on Climate Change, edited by: Solomon, S., Qin, D., Manning, M., Chen, Z., Marquis, M., Averyt, K. B., Tignor, M., and Miller, H. L., Cambridge University Press, Cambridge, United Kingdom and New York, NY, USA, 2007.

Ganzeveld, L. N., van Aardenne, J. A., Butler, T. M., Lawrence, M. G., Metzger, S. M., Stier, P., Zimmermann, P., and Lelieveld, J.: Technical Note: Anthropogenic and natural offline emissions and the online EMissions and dry DEPosition submodel EMDEP of the Modular Earth Submodel system (MESSy), Atmos. Chem. Phys. Discuss., 6, 5457–5483, doi:10.5194/acpd-6-5457-2006, 2006.

Gauss, M., Isaksen, I. S. A., Lee, D. S., and Søvde, O. A.: Impact of aircraft NO$_x$ emissions on the atmosphere – trade-offs to reduce the impact, Atmos. Chem. Phys., 6, 1529–1548, doi:10.5194/acp-6-1529-2006, 2006.

Grewe, V. and Stenke, A.: AirClim: an efficient tool for climate evaluation of aircraft technology, Atmos. Chem. Phys., 8, 4621–4639, doi:10.5194/acp-8-4621-2008, 2008.

Grewe, V., Brunner, D., Dameris, M., Grenfell, J. L., Hein, R., Shindell, D., and Staehelin, J.: Origin and variability of upper tropospheric nitrogen oxides and ozone at northern mid-latitudes, Atmos. Environ., 35, 3421–3433, 2001.

Grewe, V., Dameris, M., Fichter, C., and Sausen, R.: Impact of aircraft NO$_x$ emissions. Part 1: Interactively coupled climate-chemistry simulations and sensitivities to climate-chemistry feedback, lightning and model resolution, Meteorol. Z., 11, 177–186, 2002.

Grewe, V., Tsati, E., and Hoor, P.: On the attribution of contributions of atmospheric trace gases to emissions in atmospheric model applications, Geosci. Model Dev., 3, 487–499, doi:10.5194/gmd-3-487-2010, 2010.

Grewe, V., Dahlmann, K., Matthes, S., and Steinbrecht, W.: Attributing ozone to NO$_x$ emissions: Implications for climate mitigation measures, Atmos. Environ., 59, 102–107, 2012.

Hansen J., Sato, M., and Ruedy R.: Radiative forcing and climate response, J. Geophys. Res. 102, 6831–6864, 1997.

Holmes, C. D., Tang, Q., and Prather, M. J.: Uncertainties in climate assessment for the case of aviation NO, P. Natl. Acad. Sci. USA, 108, 10997–11002, 2011.

Hoor, P., Borken-Kleefeld, J., Caro, D., Dessens, O., Endresen, O., Gauss, M., Grewe, V., Hauglustaine, D., Isaksen, I. S. A., Jöckel, P., Lelieveld, J., Myhre, G., Meijer, E., Olivie, D., Prather, M., Schnadt Poberaj, C., Shine, K. P., Staehelin, J., Tang, Q., van Aardenne, J., van Velthoven, P., and Sausen, R.: The impact of traffic emissions on atmospheric ozone and OH: re-

sults from QUANTIFY, Atmos. Chem. Phys., 9, 3113–3136, doi:10.5194/acp-9-3113-2009, 2009.

IUPAC (see also Atkinson et al., 2004): IUPAC Subcommittee on Gas Kinetic Data Evaluation – Data Sheet HOx_VOC1, http://www.iupac-kinetic.ch.cam.ac.uk/, accessed 12 December 2011, 2007.

IUPAC: IUPAC Subcommittee on Gas Kinetic Data Evaluation – Data Sheet NOx15, http://www.iupac-kinetic.ch.cam.ac.uk/ (last access: October 2011), 2008.

Jöckel, P.: Technical note: Recursive rediscretisation of geo-scientific data in the Modular Earth Submodel System (MESSy), Atmos. Chem. Phys., 6, 3557–3562, doi:10.5194/acp-6-3557-2006, 2006.

Jöckel, P., Sander, R., Kerkweg, A., Tost, H., and Lelieveld, J.: Technical Note: The Modular Earth Submodel System (MESSy) – a new approach towards Earth System Modeling, Atmos. Chem. Phys., 5, 433–444, doi:10.5194/acp-5-433-2005, 2005.

Jöckel, P., Tost, H., Pozzer, A., Brühl, C., Buchholz, J., Ganzeveld, L., Hoor, P., Kerkweg, A., Lawrence, M. G., Sander, R., Steil, B., Stiller, G., Tanarhte, M., Taraborrelli, D., van Aardenne, J., and Lelieveld, J.: The atmospheric chemistry general circulation model ECHAM5/MESSy1: consistent simulation of ozone from the surface to the mesosphere, Atmos. Chem. Phys., 6, 5067–5104, doi:10.5194/acp-6-5067-2006, 2006.

Jöckel, P., Kerkweg, A., Buchholz-Dietsch, J., Tost, H., Sander, R., and Pozzer, A.: Technical Note: Coupling of chemical processes with the Modular Earth Submodel System (MESSy) submodel TRACER, Atmos. Chem. Phys., 8, 1677–1687, doi:10.5194/acp-8-1677-2008, 2008.

Jöckel, P., Kerkweg, A., Pozzer, A., Sander, R., Tost, H., Riede, H., Baumgaertner, A., Gromov, S., and Kern, B.: Development cycle 2 of the Modular Earth Submodel System (MESSy2), Geosci. Model Dev., 3, 717–752, doi:10.5194/gmd-3-717-2010, 2010.

Kärcher, B. and Voigt, C.: Formation of nitric acid/water ice particles in cirrus clouds. Geophys. Res. Lett., 33, L08806, doi:10.1029/2006GL025927, 2006.

Kanno, M., Tonukura, K., and Koshi, M.: Equilibrium constant of the HO$_2$-H$_2$O complex formation and kinetics of HO$_2$ + HO$_2$-H$_2$O: Implications for tropospheric chemistry, J. Geophys. Res., 111, D20312, doi:10.1029/2005JD006805, 2006.

Kawa, S. R., Anderson, J. G., Baughcum, S. L., Brock, C. A., Brune, W. H., Cohen, R. C., Kinnison, D. E., Newman, P. A., Rodriguez, J. M., Stolarski, R. S., Waugh, D., and Wofsy, S. C.: Assessment of the Effects of High-Speed Aircraft in the Stratosphere 1998, Technical report, NASA, nASA TP-1999-209237, 1998.

Kerkweg, A.: Global Modelling of Atmospheric Halogen Chemistry in the Marine Boundary Layer, Ph.D. thesis, University of Bonn, Germany, http://hss.ulb.uni-bonn.de/2005/0636/0636.htm, 2005.

Kerkweg, A., Buchholz, J., Ganzeveld, L., Pozzer, A., Tost, H., and Jöckel, P.: Technical Note: An implementation of the dry removal processes DRY DEPosition and SEDImentation in the Modular Earth Submodel System (MESSy), Atmos. Chem. Phys., 6, 4617–4632, doi:10.5194/acp-6-4617-2006, 2006a.

Kerkweg, A., Sander, R., Tost, H., and Jöckel, P.: Technical note: Implementation of prescribed (OFFLEM), calculated (ON-LEM), and pseudo-emissions (TNUDGE) of chemical species in the Modular Earth Submodel System (MESSy), Atmos. Chem. Phys., 6, 3603–3609, doi:10.5194/acp-6-3603-2006, 2006b.

Kirner, O., Ruhnke, R., Buchholz-Dietsch, J., Jöckel, P., Brühl, C., and Steil, B.: Simulation of polar stratospheric clouds in the chemistry-climate-model EMAC via the submodel PSC, Geosci. Model Dev., 4, 169–182, doi:10.5194/gmd-4-169-2011, 2011.

Köhler, M., Rädel, G., Dessens, O., Shine, K., Rogers, H., Wild, O., and Pyle, J.: Impact of perturbations to nitrogen oxide emissions from global aviation, J. Geophys. Res., 113, D11305, doi:10.1029/2007JD009140, 2008.

Kvalevåg, M. M. and Myhre, G.: Human impact on direct and diffuse solar radiation during the industrial era, J. Climate, 20, 4874–4883, 2007.

Lamarque, J.-F., Bond, T. C., Eyring, V., Granier, C., Heil, A., Klimont, Z., Lee, D., Liousse, C., Mieville, A., Owen, B., Schultz, M. G., Shindell, D., Smith, S. J., Stehfest, E., Van Aardenne, J., Cooper, O. R., Kainuma, M., Mahowald, N., McConnell, J. R., Naik, V., Riahi, K., and van Vuuren, D. P.: Historical (1850–2000) gridded anthropogenic and biomass burning emissions of reactive gases and aerosols: methodology and application, Atmos. Chem. Phys., 10, 7017–7039, doi:10.5194/acp-10-7017-2010, 2010.

Lawrence, M. G., Jöckel, P., and von Kuhlmann, R.: What does the global mean OH concentration tell us?, Atmos. Chem. Phys., 1, 37–49, doi:10.5194/acp-1-37-2001, 2001.

Le Bras, G.: Interactive comment on "The HNO$_3$ forming branch of the HO$_2$+ NO reaction: pre-industrial-to-present trends in atmospheric species and radiative forcings", Atmos. Chem. Phys. Discuss., 11, C5228–C5229, 2011.

Lee, D. S., Owen, B., Graham, A., Fichter, C., Lim, L. L., and Dimitriu, D.: Allocation of International Aviation Emissions from Scheduled Air Traffic – Present Day and Historical, Final Report to DEFRA Global Atmosphere Division, Manchester Metropolitan University, Centre for Air Transport and the Environment, Manchester, UK, 2005.

Lee, D. S., Fahey, D. W., Forster, P. M., Newton, P. J., Wit, R. C. N., Lim, L. L., Owen, B., and Sausen, R.: Aviation and global climate change in the 21st century, Atmos. Environ., 43, 3520–3537, 2009.

Lee D. S., Pitari, G., Grewe, V., Gierens, K., Penner, J. E., Petzold, A., Prather, M. J., Schumann, U., Bais, A., Berntsen, T., Iachetti, D., Lim, L. L., and Sausen, R.: Transport impacts on atmosphere and climate: Aviation, Atmos. Environ., 44, 4678–4734, 2010.

Lin, X., Trainer, M., and Liu, S. C.: On the nonlinearity of the tropospheric ozone production, J. Geophys. Res. 93, 15879–15888, 1988.

Lohmann, U. and Roeckner, E.: Design and performance of a new cloud microphysics scheme developed for the ECHAM general circulation model, Clim. Dynam., 12, 557–572, 1996.

Montzka, S. A., Krol, M., Dlugokencky, E., Hall, B., Jöckel, P., and Lelieveld, J.: Small interannual variability of global atmospheric hydroxyl, Science, 331, 67–69, 2011.

Müller, D. J.-F.: Interactive comment on "The HNO$_3$ forming branch of the HO$_2$+ NO reaction: pre-industrial-to-present trends in atmospheric species and radiative forcings", Atmos. Chem. Phys. Discuss., 11, C5228–C5229, doi:10.5194/acpd-11-C5228-2011, 2011.

Myhre, G., Nilsen, J. S., Gulstad, L., Shine, K. P., Rognerud, B., and Isaksen, I. S. A.: Radiative forcing due to stratospheric water vapour from CH$_4$ oxidation, Geophys. Res. Lett., 34, L01807, doi:10.1029/2006GL027472, 2007.

Myhre, G., Shine, K. P., Rädel, G., Gauss, M., Isaksen, I. S. A., Tang, Q., Prather, M. J., Williams, J. E., van Velthoven, P., Dessens, O., Koffi, B., Szopa S., Hoor, P., Grewe, V., Borken-Kleefeld, J., Berntsen, T. K., and Fuglestvedt, J. S.: Radiative forcing due to changes in ozone and methane caused by the transport sector, Atmos. Environ., 45, 387–394, 2011.

Penner, J. E., Lister, D. H., Griggs, D. J., Dokken, D. J., and Mc-Farland, M. (Eds.): Aviation and the global atmosphere – A special report of IPCC working groups I and III. Intergovernmental Panel on Climate Change, Cambridge University Press, Cambridge, United Kingdom and New York, NY, USA, 373 pp., 1999.

Pozzer, A., Jöckel, P., Sander, R., Williams, J., Ganzeveld, L., and Lelieveld, J.: Technical Note: The MESSy-submodel AIRSEA calculating the air-sea exchange of chemical species, Atmos. Chem. Phys., 6, 5435–5444, doi:10.5194/acp-6-5435-2006, 2006.

Prather, M. J., Holmes, C. D., and Hsu, J.: Reactive greenhouse gas scenarios: Systematic exploration of uncertainties and the role of atmospheric chemistry, Geophys. Res. Lett., 39, L09803, doi:10.1029/2012GL051440, 2012.

QUANTIFY: Global gridded aircraft and road emissions, present, downloaded from http://srb.uio.no/mySRB/UIO/home/quantify.SRBuio/Quantify-a3/emis_present, /aircraft_final/QTF_2000_Scaled.nc, 1 June 2008, modified for use with EMAC, /road_final/*.nc, 5 June 2008, data now at http://www.pa.op.dlr.de/quantify, 2008.

Ramaswamy, V., Boucher, O., Haigh, J., Hauglustaine, D., Haywood, J., Myhre, G., Nakajima, T., Shi, G. Y., and Solomon, S.: Radiative forcing of climate change, in Climate Change 2001: The Scientific Basis. Contribution of Working Group I to the Third Assessment Report of the Intergovernmental Panel on Climate Change, edited by: Houghton, J. T., Ding, Y., Griggs, D. J., Noguer, M., van der Linden, P. J., Dai, X., Maskell, K., and Johnson, C. A., Cambridge University Press, Cambridge, United Kingdom and New York, NY, USA, 351–416, 2001.

Roeckner, E., Bäuml, G., Bonaventura, L., Brokopf, R., Esch, M., Giorgetta, M., Hagemann, S., Kirchner, I., Kornblueh, L., Manzini, E., Rhodin, A., Schlese, U., Schulzweida, U., and Tompkins, A.: The atmospheric general circulation model ECHAM5. PART I: Model description, Technical report, Max Planck Institute for Meteorology, MPI-Report 349, http://www.mpimet.mpg.de/fileadmin/publikationen/Reports/max_scirep_349.pdf, 2003.

Roeckner, E., Brokopf, R., Esch, M., Giorgetta, M., Hagemann, S., Kornblueh, L., Manzini, E., Schlese, U., and Schulzweida, U.: Sensitivity of simulated climate to horizontal and vertical resolution in the ECHAM5 atmosphere model, J. Climate, 19, 3771–3791, 2006.

Sander, R., Kerkweg, A., Jöckel, P., and Lelieveld, J.: Technical note: The new comprehensive atmospheric chemistry module MECCA, Atmos. Chem. Phys., 5, 445–450, doi:10.5194/acp-5-445-2005, 2005.

Sander, S. P., Finlayson-Pitts, B. J., Friedl, R. R., Golden, D. M., Huie, R. E., Kolb, C. E., Kurylo, M. J., Molina, M. J., Moortgat, G. K., Orkin, V. L., and Ravishankara, A. R.: Chemical Kinetics and Photochemical Data for Use in Atmospheric Studies, Evaluation Number 14, JPL Publication 02-25, Jet Propulsion Laboratory, Pasadena, CA, 2003.

Sander, S. P., Barker, J. R., Golden, D. M., Kurylo, M. J., and Wine, P. H.: Chemical Kinetics and Photochemical Data for Use in Atmospheric Studies, Evaluation Number 17, JPL Publication 10-6, Jet Propulsion Laboratory, Pasadena, CA, 2011.

Schreiner J., Voigt, C., Kohlmann, A., Arnold, F., Mauersberger, K., and Larsen, N.: Chemical analysis of polar stratospheric cloud particles, Science, 283, 968–970, 1999.

Schumann, U. and Huntrieser, H.: The global lightning-induced nitrogen oxides source, Atmos. Chem. Phys., 7, 3823–3907, doi:10.5194/acp-7-3823-2007, 2007.

Shindell, D. T., Faluvegi, G., Stevenson, D. S., Krol, M. C., Emmons, L. K., Lamarque, J.-F., Pétron, G., Dentener, F. J., Ellingsen, K., Schultz, M. G., Wild, O., Amann, M., Atherton, C. S., Bergmann, D. J., Bey, I., Butler, T., Cofala, J., Collins, W. J., Derwent, R.G., Doherty, R. M., Drevet, J., Eskes, H. J., Fiore, A. M., Gauss, M., Hauglustaine, D. A., Horowitz, L. W., Isaksen, I. S. A., Lawrence, M. G., Montanaro, V., Müller, J. F., Pitari, G., Prather, M. J., Pyle, J. A., Rast, S., Rodriguez, J. M., Sanderson, M. G., Savage, N. H., Strahan, S. E., Sudo, K., Szopa, S., Unger, N., van Noije, T. P. C., and Zeng, G.: Multimodel simulations of carbon monoxide: Comparison with observations and projected near-future changes, J. Geophys. Res., 111, D19306, doi:10.1029/2006JD007100, 2006.

Søvde, O. A., Gauss, M., Isaksen, I. S. A., Pitari, G., and Marizy, C.: Aircraft pollution – a futuristic view, Atmos. Chem. Phys., 7, 3621–3632, doi:10.5194/acp-7-3621-2007, 2007.

Søvde, O. A., Hoyle, C. R., Myhre, G., and Isaksen, I. S. A.: The HNO$_3$ forming branch of the HO$_2$ + NO reaction: pre-industrial-to-present trends in atmospheric species and radiative forcings, Atmos. Chem. Phys., 11, 8929–8943, doi:10.5194/acp-11-8929-2011, 2011.

Spiro, P. A., Jacob, D. J., and Logan, J. A.: Global Inventory of Sulfur Emissions With 1_×1_Resolution, J. Geophys. Res., 97, 6023–6036, 1992.

Spivakovsky, C. M., Logan, J. A., Montzka, S. A., Balkanski, Y. J., Foreman-Fowler, M., Jones, D. B. A., Horowitz, L. W., Fusco, A. C., Brenninkmeijer, C. A. M., Prather, M. J.,Wofsy, S. C., and McElroy, M. B.: Three-dimensional climatological distribution of tropospheric OH: Update and evaluation, J. Geophys. Res., 105, 8931–8980, 2000.

Stenke, A., Deckert, R., and Gottschaldt, K.: Methane modeling – from process-oriented models to global climate models, in: Atmospheric Physics – Background – Methods – Trends, edited by: Schumann, U., Springer, 781–797, doi:10.1007/978-3-642-30183-4, 2012.

Stevenson, D. S., Dentener, F. J., Schultz, M. G. , Ellingsen, K., van Noije, T. P. C., Wild, O., Zeng, G., Amann, M., Atherton, C. S., Bell, N., Bergmann, D. J., Bey, I., Butler, T., Cofala, J., Collins, W. J., Derwent, R. G., Doherty, R. M., Drevet, J., Eskes, H. J., Fiore, A. M., Gauss, M., Hauglustaine, D. A., Horowitz, L. W., Isaksen, I. S. A., Krol, M. C., Lamarque, J.-F., Lawrence, M. G., Montanaro, V., Müller, J.-F., Pitari, G., Prather, M. J., Pyle, J. A., Rast, S., Rodriguez, J. M., Sanderson, M. G., Savage, N. H., Shindell, D. T., Strahan, S. E., Sudo, K., and Szopa, S.: Multimodel ensemble simulationsof present-day and near-future tropospheric ozone, J. Geophys. Res., 111, D08301, doi:10.1029/2005JD006338, 2006.

Stuber, N., Sausen, R., and Ponater, M.: Stratosphere adjusted radiative forcing in a comprehensive climate model, Theor. Appl.

Climatol., 68, 125–135, 2001.

Sundqvist, H.: A parameterization scheme for non-convective condensation including prediction of cloud water content, Q. J. Roy. Meteor. Soc., 104, 677–690, 1978.

Tanre, D., Geleyn, J.-F., and Slingo, J. M.: First results of the introduction of an advanced aerosol-radiation interaction in the ECMWF low resolution global model, in: Aerosols and their climatic effects, edited by: Gerber, H. and Deepak, A., 133–177, A. Deepak, Hampton, VA, 1984.

Taraborrelli, D., Lawrence, M. G., Crowley, J. N., Dillon, T. J., Gromov, S., Groß, C. B. M., Vereecken, L., and Lelieveld, J.: Hydroxyl radical buffered by isoprene oxidation over tropical forests, Nat. Geosc., 5, 190–193, doi:10.1038/ngeo1405, 2012.

Tost, H., Jöckel, P., Kerkweg, A., Sander, R., and Lelieveld, J.: Technical note: A new comprehensive SCAVenging submodel for global atmospheric chemistry modelling, Atmos. Chem. Phys., 6, 565–574, doi:10.5194/acp-6-565-2006, 2006a.

Tost, H., Jöckel, P., and Lelieveld, J.: Influence of different convection parameterisations in a GCM, Atmos. Chem. Phys., 6, 5475–5493, doi:10.5194/acp-6-5475-2006, 2006b.

Tost, H., Jöckel, P., Kerkweg, A., Pozzer, A., Sander, R., and Lelieveld, J.: Global cloud and precipitation chemistry and wet deposition: tropospheric model simulations with ECHAM5/MESSy1, Atmos. Chem. Phys., 7, 2733–2757, doi:10.5194/acp-7-2733-2007, 2007.

Tost, H., Lawrence, M. G., Brühl, C., Jöckel, P., The GABRIEL Team, and The SCOUT-O3-DARWIN/ACTIVE Team: Uncertainties in atmospheric chemistry modelling due to convection parameterisations and subsequent scavenging, Atmos. Chem. Phys., 10, 1931–1951, doi:10.5194/acp-10-1931-2010, 2010.

Unger, N.: Global climate impact of civil aviation for standard and desulfurized jet fuel, Geophys. Res. Lett., 38, L20803, doi:10.1029/2011GL049289, 2011.

Unger, N., Shindell, D. T., Koch, D. M., and Streets, D. G.: Cross influences of ozone and sulfate precursor emissions changes on air quality and climate, P. Natl. Acad. Sci. USA, 103, 4377–4380, doi:10.1073/pnas.0508769103, 2006.

van Aardenne, J., Dentener, F., Olivier, J., Peters, J., and Ganzeveld, L.: The EDGAR3.2 Fast Track 2000 data set (32FT2000), Joint Research Center, Institute for Environment and Sustainability (JRC-IES), Climate Change Unit, TP280, 21020 Ispra, Italy, 2005.

van der Werf, G. R., Randerson, J. T., Giglio, L., Collatz, G. J., Mu, M., Kasibhatla, P. S., Morton, D. C., DeFries, R. S., Jin, Y., and van Leeuwen, T. T.: Global fire emissions and the contribution of deforestation, savanna, forest, agricultural, and peat fires (1997–2009), Atmos. Chem. Phys., 10, 11707–11735, doi:10.5194/acp-10-11707-2010, 2010.

Voigt, C., Tsias, S., Dörnbrack, A., Meilinger, S., Luo, B. P., Schreiner, J., Larsen, N., Mauersberger, K., and Peter, T.: Non-equilibrium compositions of liquid polar stratospheric clouds in gravity waves, Geophys. Res. Lett., 27, 3873–3876, doi:10.1029/2000GL012168, 2000.

Voigt C., Schlager, H., Ziereis, H., Kärcher, B., Luo, B. P., Schiller, C., Krämer, M., Popp, P. J., Irie, H., and Kondo, Y.: Nitric acid in cirrus clouds, Geophys. Res. Lett., 33, L05803, doi:10.1029/2005GL025159, 2006.

Voigt, C., Kärcher, B., Schlager, H., Schiller, C., Krämer, M., de Reus, M., Vössing, H., Borrmann, S., and Mitev, V.: In-situ observations and modeling of small nitric acid-containing ice crystals, Atmos. Chem. Phys., 7, 3373–3383, doi:10.5194/acp-7-3373-2007, 2007.

von Kuhlmann, R.: Photochemistry of Tropospheric Ozone, its Precursors and the Hydroxyl radical: A 3D-Modeling Study Considering Non-Methane Hydrocarbons, Ph.D. thesis, University of Mainz, Germany, 2001.

von Kuhlmann, R., Lawrence, M. G., Crutzen, P. J., and Rasch, P. J.: A model for studies of tropospheric ozone and nonmethane hydrocarbons: Model evaluation of ozone-related species, J. Geophys. Res., 108, 4729, doi:10.1029/2002JD003348, 2003.

Wennberg, P. O., Hanisco, T. F., Jaegle, L., Jacob, D. J., Hintsa, E. J., Lanzendorf, E. J., Anderson, J. G., Gao, R.-S., Keim, E. R., Donnelly, S. G., Del Negro, L. A., Fahey, D. W., McKeen, S. A., Salawitch, R. J., Webster, C. R., May, R. D., Herman, R. L., Proffitt, M. H., Margitan, J. J., Atlas, E. L., Schauffler, S. M., Flocke, F., McElroy, C. T., and Bui, T. P.: Hydrogen Radicals, Nitrogen Radicals, and the Production of O$_3$ in the Upper Troposphere, Science 279, 49–53, 1998.

WMO: International meteorological vocabulary, 2nd ed., ISBN 92-63-02182-1, Secretariat of the World Meteorological Organization, Geneva, Switzerland, 1992.

Wu, S. L., Duncan, B. N., Jacob, D. J., Fiore, A. M., and Wild, O.: Chemical nonlinearities in relating intercontinental ozone pollution to anthropogenic emissions, Geophys. Res. Lett., 36, L05806, doi:10.1029/2008GL036607, 2009.

Zhang, J. and Donanhue, N. M.: Constraining the Mechanism and Kinetics of OH + NO$_2$ and HO$_2$ + NO Using the Multiple-Well Master Equation, J. Phys. Chem. A, 110, 6898–6911, 2006.